Chemical Geology 466 (2017) 239–255

Contents lists available at ScienceDirect

Chemical Geology

journal homepage: www.elsevier.com/locate/chemgeo

Revised Middle–Upper Jurassic strontium isotope stratigraphy

Hubert Wierzbowski[a,*], Robert Anczkiewicz[b], Jacek Pawlak[c], Mikhail A. Rogov[d], Anton B. Kuznetsov[e]

[a] Polish Geological Institute – National Research Institute, ul. Rakowiecka 4, PL 00-975 Warsaw, Poland
[b] Institute of Geological Sciences, Polish Academy of Sciences, ul. Senacka 1, PL 31-002 Cracow, Poland
[c] Institute of Geological Sciences, Polish Academy of Sciences, ul. Twarda 51/55, PL 00-818 Warsaw, Poland
[d] Geological Institute, Russian Academy of Sciences, Pyzhevsky lane 7, 119017 Moscow, Russia
[e] Institute of Precambrian Geology and Geochronology, Russian Academy of Sciences, nab. Makarova 2, St. Petersburg 199034, Russia

ARTICLE INFO

Keywords:
Aalenian–Tithonian
Belemnites
Strontium isotopes
Seawater $^{87}Sr/^{86}Sr$ ratio
Activity of the oceanic crust

ABSTRACT

A study is conducted to supplement the uppermost Lower Jurassic–lowermost Cretaceous marine strontium isotope dataset and to present new statistical fits of the Middle–Late Jurassic seawater strontium isotope curve based on a numerical time scale and a detailed biostratigraphical zonal scheme. The use of the stratigraphical scheme allows reduction of dating errors related to uncertainty of numerical age determinations. The presented correlation charts enable direct calibration between strontium isotope stratigraphy and regional biostratigraphical frameworks. New strontium isotope data have been obtained from well-preserved Lower Bajocian, uppermost Callovian, Oxfordian, Kimmeridgian, and Upper Volgian belemnite rostra.

The presented seawater $^{87}Sr/^{86}Sr$ curve is characterized by reliable 95% confidence limits (mean width of ± 0.000007), which take into account precision of dating of particular data points. A decrease of seawater $^{87}Sr/^{86}Sr$ ratio, from ca. 0.70730 to ca. 0.70683, is observed throughout the Middle Aalenian–Early Oxfordian (172.1–160.8 Ma ago). The steepest Phanerozoic fall of the ratio, with a rate of change of up to 0.00015 per 1 Ma, is recorded in the Bajocian segment of the strontium isotope curve. The Phanerozoic minimum of the marine $^{87}Sr/^{86}Sr$ ratio occurred at the Early–Middle Oxfordian transition. The $^{87}Sr/^{86}Sr$ ratio increased starting from the Middle Oxfordian till the end of the Jurassic (160.8–145.7 Ma) reaching a value of ca. 0.70720 at the Jurassic–Cretaceous transition. The Middle–earliest Late Jurassic decrease in seawater $^{87}Sr/^{86}Sr$ ratio is interpreted as a result of the increased hydrothermal activity of the seafloor during the breakup of Gondwana, and the formation of new Atlantic–Tethyan oceanic basins. The successive rise of the ratio is probably related to the decelerated hydrothermal venting of the oceanic crust although a partial increase in radiogenic strontium input from continental weathering cannot be excluded.

1. Introduction

Strontium isotope composition of seawater and most polyhaline brackish waters is uniform due to high strontium concentrations, long residence time of strontium in oceans (1 to $5 * 10^6$ years), and short mixing time of oceanic water masses (1 to $1.5 * 10^3$ years; cf. Elderfield, 1986; Faure, 1986; McArthur, 1994; Bryant et al., 1995; Basu et al., 2001; Jones and Jenkyns, 2001; Krabbenhöft et al., 2010; Kuznetsov et al., 2012; Wierzbowski, 2013). The seawater strontium isotope composition has varied during geologic history of the Earth owing to changing inputs of strontium from three major sources. Non-radiogenic strontium of low $^{87}Sr/^{86}Sr$ ratios (~0.703) is delivered by hydrothermal fluids from oceanic ridges and hot spots, radiogenic strontium of high $^{87}Sr/^{86}Sr$ ratios (~0.711) is contributed by rivers, and groundwater from continental weathering, and strontium of intermediate $^{87}Sr/^{86}Sr$ ratios (~0.709) is derived from submarine dissolution and re-crystallization of sediments (cf. Elderfield, 1986; Faure, 1986; McArthur, 1994; Jones and Jenkyns, 2001; Davis et al., 2003; Krabbenhöft et al., 2010; Peucker-Ehrenbrink et al., 2010; Wierzbowski, 2013; Pearce et al., 2015).

Normalization procedure used during strontium isotope measurements (cf. Nier, 1938; Korte and Ullmann, in press) removes any effects of biological fractionation and laboratory purification methods on the $^{87}Sr/^{86}Sr$ ratio of carbonates and phosphates. Therefore, marine carbonates and phosphates can be used as a direct proxy for the strontium isotope composition of ancient seawater.

A temporal seawater strontium isotope curve shows several maxima and minima. The Middle–Late Jurassic part of the curve is characterized

* Corresponding author.
E-mail address: hubert.wierzbowski@pgi.gov.pl (H. Wierzbowski).

http://dx.doi.org/10.1016/j.chemgeo.2017.06.015
Received 6 April 2017; Received in revised form 6 June 2017; Accepted 14 June 2017
Available online 16 June 2017

by very low $^{87}Sr/^{86}Sr$ ratios, and comprises the deepest Phanerozoic trough of the curve (cf. McArthur et al., 2012; Korte and Ullmann, in press). The Middle–Late Jurassic strontium-isotope trends based on data from well-preserved belemnite rostra and oyster shells are presented by Jones et al. (1994b), Jenkyns et al. (2002), and McArthur et al. (2001, 2012). The published Jurassic strontium isotope trends show different scatter of data points, and temporal resolution; the curve of McArthur et al. (2001, 2012), which is established on the basis of statistical methods, is characterized by the highest resolution, and given 95% confidence limits.

The Middle–Upper Jurassic strontium isotope stratigraphy has a great potential because of significant variations in the seawater $^{87}Sr/^{86}Sr$ ratios, common occurrences of well-preserved belemnite rostra and oyster shells, and its potential applicability to dating of hydrocarbon source rocks. Since high-resolution Middle–Late Jurassic strontium isotope curve of McArthur et al. (2001, 2012) is related to absolute time frames only, direct data translation into standard biostratigraphical units may, however, introduce some errors related to uncertainty of radiogenic dating, and gradual modifications of accepted numerical ages of stage boundaries (cf. Gradstein, 2012). In addition, crucial strontium isotope data are still lacking for the Oxfordian–Kimmeridgian, and some other intervals of the Middle–Upper Jurassic, which makes difficulties in the precise determination of seawater strontium isotope ratios during these periods.

The current study aims at the presentation of new, reliable strontium isotope data from poorly studied intervals, and the construction of the high-resolution Middle–Late Jurassic seawater strontium isotope curve, which is based on both the numerical time scale of the Jurassic, and the detailed biostratigraphical zonal scheme. Dating errors of the curve based on the stratigraphical scheme are limited due to direct calibration to regular ammonite units. In addition, interregional correlation charts are presented to allow biostratigraphical dating of deposits from various biogeoprovinces, where regional ammonite zonal schemes are applied.

2. Material

New strontium isotope analyses of archival and newly collected belemnite rostra have been conducted to obtain additional data points for the calibration of the Middle–Late Jurassic strontium isotope curve. Archival materials, studied previously for oxygen and carbon isotope compositions, are derived from the Smolegowa Limestone Formation of the Kamienka section in the Pieniny Klippen Belt, northern Slovakia (Lower Bajocian; cf. Segit, 2010; Arabas, 2016), from the Jasna Góra and the Zawodzie limestone members of the Częstochowa Sponge Limestone Formation, which outcrop in several sections in the Polish Jura Chain, central Poland (uppermost Callovian–lowermost Kimmeridgian; cf. Wierzbowski, 2002, 2015; Wierzbowski et al., 2014), from the Impressamergel and the Wohlgeschichteten-Kalken formations of the Plettenberg section in the Swabian Alb, southern Germany (lowermost Kimmeridgian; Schweigert and Callomon, 1997, Wierzbowski, 2004, 2015; Wierzbowski et al., 2014), and from clays of the Mikhalenino section, Kostroma Region, Russian Platform (Lower Kimmeridgian; Głowniak et al., 2010; Wierzbowski et al., 2013; Table 1). New strontium isotope measurements of samples from the Jurassic–Cretaceous boundary interval of the Maurynya section (Western Siberia) are also presented (cf. Shurygin et al., 2015; for position of data points, and trace element contents see Dzyuba et al., 2013, and Table 1).

New belemnite samples have been collected from clays and marls of the Tarkhanovskaya Pristan' section, Tatarstan, Russian Platform (Lower–Upper Kimmeridgian boundary), and the Karamyshevskaya Naberezhnaya section, Moscow, Russian Platform (Upper Volgian; Table 1). The biostratigraphy of the Tarkhanovskaya Pristan' section has been studied by Shchepetova and Rogov (2013), Rogov et al. (2014), and Rogov et al. (in press). The section comprises Lower–Upper Kimmeridgian boundary beds (Divisum and Mutabilis zones). The biostratigraphy of the Karamyshevskaya Naberezhnaya section has been studied, in details, by Rogov and Starodubtseva (2014). The section comprises the Middle–Upper Volgian (Virgatus to Catenulatum zones).

The new strontium isotope dataset has been supplemented with published data of Jones et al. (1994a, 1994b), Callomon and Dietl (2000), McArthur et al. (2000), Jenkyns et al. (2002), Gröcke et al. (2003), McArthur et al. (2007), Page et al. (2009), and Wierzbowski et al. (2012), all of which are derived from well-preserved and stratigraphically well-dated belemnite rostra and oyster shells.

3. Methodology

Thin sections prepared from newly collected belemnite rostra were studied by means of cold-cathode cathodoluminescence microscopy. The rostra were cleaned, using a microdrill, from adherent sediment, apical-line areas, alveolar fissure infillings and, if necessary, narrow luminescent rims (cf. Wierzbowski and Joachimski, 2007; Wierzbowski et al., 2009; Wierzbowski, 2015). Fragments of newly studied belemnite rostra comprising most growth rings, and derived from the *rostrum solidum* (cf. Sælen, 1989) were powdered and homogenized to get average isotope values (the sample size was 100–300 mg). Aliquots of the same carbonate powders were used for chemical and strontium isotope analyses.

Ca, Mn, Fe, and Sr concentrations were determined by the ICP-OES (Inductively Coupled Plasma Optical Emission Spectrometry) method using Thermo iCAP 6500 Duo system in the Polish Geological Institute–National Research Institute in Warsaw after dissolving the carbonate powders in 5% (v/v) hydrochloric acid. Reproducibility of chemical analyses (2 SD) was controlled by multiple analyses of measured samples and averages 1.0% for Ca, 0.8% for Mn, 2.7% for Fe, and 2.2% for Sr. Repeated analyses of calcite and dolomite reference materials: JLs-1 and JDo-1 (cf. Imai et al., 1996) gave accuracy of measurements better than 3.5% for Ca, 4.0% for Mn, and 1.0% for Sr. The accuracy of Fe analyses cannot be given precisely owing to the employed dissolution method in weak hydrochloric acid, which is not relevant for the determination of non-carbonate iron compounds present in both references.

Analyses of strontium isotope composition of 50 archival and new samples were performed at the Cracow Research Centre, Institute of Geological Sciences, Polish Academy of Sciences. Powdered belemnite rostra were dissolved in 0.5 M acetic acid. After dissolution, samples were centrifuged and solution was evaporated to dryness. Strontium was separated from matrix in two steps by means of ion exchange chromatography. Initial purification took place on an ion-exchange resin (Bio-Rad 50 W-X8), which was followed by separation on a Sr-spec resin (Eichrom). The purified strontium fraction was evaporated and re-dissolved in 2% HNO_3 for mass spectrometric analyses. Measurements were carried out using the multi collector ICP-MS Neptune in a static mode. Instrumental mass bias was corrected using $^{86}Sr/^{88}Sr$ ratio of 0.1194 applying exponential law (cf. Nier, 1938; Russell et al., 1978). Reproducibility of $^{87}Sr/^{86}Sr$ ratio of SRM 987 reference standard over two periods of analyses, in years 2014 and 2016, were 0.710260 ± 0.000012 ($n = 11$), and 0.710254 ± 0.000006 ($n = 9$), respectively. Errors are given as two standard deviations (SD). The obtained results were normalized to the recommended SRM 987 $^{87}Sr/^{86}Sr$ ratio of 0.710248 (McArthur, 1994; McArthur et al., 2001, 2012). Total strontium blank was below 20 pg compared to > 20 µg strontium in analysed samples, and thus its influence on the measured isotopic ratios was negligible.

Strontium isotope analyses of 23 belemnite rostra, collected at the Western Siberian section (see Dzyuba et al., 2013; Shurygin et al., 2015), were carried out at laboratory of the Institute of Precambrian Geology and Geochronology, Russian Academy of Sciences. Sample fragments were cleaned in ultrasonic bath with deionized water, and subsequently dissolved in 0.5 N HCl (cf. Kuznetsov et al., 2012).

Table 1
Stratigraphy, age, chemical data and strontium isotope composition of newly studied belemnite rostra, used for the construction of the Middle–Late Jurassic marine $^{87}Sr/^{86}Sr$ curve. Position – "biostratigraphical age" calculated, starting from the base of the studied succession, assuming equal duration of ammonite subchrons (see Fig. 1).

Sample	$^{87}Sr/^{86}Sr$ measured	2 s.e.	$^{87}Sr/^{86}Sr$ normal.	Position	(Sub)zone	Age (Ma)	Ca (ppm)	Mn (ppm)	Fe (ppm)	Sr (ppm)	Mn/Ca * 1000	Fe/Ca * 1000	Sr/Ca * 1000
Strontium isotope data from southern Germany (cf. Wierzbowski et al., 2014)													
HW70[a]	0.706871	0.000009	0.706871	80.60	Planula	156.53	31.2	6	61	1093	0.01	0.14	1.60
HW74[a]	0.706895	0.000009	0.706881	80.30	Planula	156.64	35.2	6	6	1395	0.01	0.01	1.81
HW67[a]	0.706893	0.000014	0.706879	80.00	Planula/Hauffianum	156.75	37	9	27	1003	0.02	0.05	1.24
Strontium isotope data from central Poland (cf. Wierzbowski et al., 2014)													
HW103[b]	0.706850	0.000009	0.706850	77.34	Hypselum	158.12	36.1	13	< 20	948	0.03	< 0.04	1.20
HW101[b]	0.706849	0.000009	0.706849	77.14	Hypselum	158.37	36	8	< 20	1005	0.02	< 0.04	1.28
HW 100[b]	0.706879	0.000011	0.706865	77.00	Hypselum/Grossouvrei	158.54	35.4	12	31	982	0.02	0.06	1.27
HW79[b]	0.706879	0.000010	0.706865	76.71	Grossouvrei	158.63	38.7	5	< 20	999	0.01	< 0.04	1.18
HW108[b]	0.706879	0.000011	0.706865	76.43	Grossouvrei	158.71	35.8	3	< 20	1025	0.01	< 0.04	1.31
HW78[b]	0.706868	0.000012	0.706854	74.50	Wartae	159.29	38.6	5	< 20	1041	0.01	< 0.04	1.23
HW13[b]	0.706850	0.000010	0.706836	72.36	Buckmani	160.07	36.9	4	38	1002	0.01	0.07	1.24
HW73[b]	0.706820	0.000012	0.706820	71.84	Arkelli	160.24	37.9	23	60	1047	0.04	0.11	1.26
HW64[b]	0.706832	0.000010	0.706832	71.24	Arkelli	160.37	37.6	5	31	1061	0.01	0.06	1.29
HW60[b]	0.706819	0.000010	0.706819	71.00	Arkelli/Ouatius	160.42	35.2	15	42	1060	0.03	0.09	1.38
HW84[b]	0.706846	0.000009	0.706832	70.36	Ouatius	160.55	37.9	11	50	1026	0.02	0.09	1.24
HW44[b]	0.706813	0.000008	0.706813	70.36	Ouatius	160.55	37.8	6	< 20	991	0.01	< 0.04	1.20
HW76[b]	0.706841	0.000011	0.706827	70.07	Ouatius	160.62	36.4	4	28	1197	0.01	0.06	1.50
HW75[b]	0.706845	0.000012	0.706831	70.07	Ouatius	160.62	36.4	5	55	992	0.01	0.11	1.25
HW85[b]	0.706840	0.000014	0.706826	69.86	Paturattensis	160.66	36.1	20	115	989	0.04	0.23	1.25
HW142[a]	0.706841	0.000010	0.706827	69.43	Paturattensis	160.75	37.1	27	27	1086	0.05	0.05	1.34
HW63[c]	0.706847	0.000009	0.706833	68.50	Cordatum	160.93	36.2	37	68	1056	0.07	0.13	1.33
HW89[c]	0.706842	0.000011	0.706828	68.50	Cordatum	160.93	38.2	9	49	1064	0.02	0.09	1.27
HW88[c]	0.706853	0.000011	0.706840	68.07	Cordatum	161.01	37.9	29	50	1091	0.06	0.09	1.32
HW222[c]	0.706836	0.000012	0.706822	67.90	Costicardia	161.04	38.1	10	25	1151	0.02	0.05	1.38
HW223[c]	0.706838	0.000012	0.706824	67.50	Costicardia	161.12	37.8	15	33	1160	0.03	0.06	1.40
HW290[c]	0.706834	0.000009	0.706820	67.15	Costicardia	161.18	37.5	37	18	1096	0.07	0.03	1.34
HW293[c]	0.706839	0.000012	0.706825	66.90	Bukowskii	161.23	37.3	10	10	1126	0.02	0.02	1.38
HW292[c]	0.706842	0.000012	0.706828	66.80	Bukowskii	161.25	38.5	9	21	1311	0.02	0.04	1.56
HW288[c]	0.706846	0.000010	0.706832	66.45	Bukowskii	161.31	37.3	26	62	1025	0.05	0.12	1.26
HW90[c]	0.706833	0.000010	0.706819	66.43	Bukowskii	161.31	36.1	22	38	1043	0.04	0.08	1.32
KSP5[b]	0.706855	0.000014	0.706841	63.83	Lamberti	163.16	37.2	3	< 20	1057	0.01	< 0.04	1.30
KSP3[b]	0.706877	0.000011	0.706863	63.83	Lamberti	163.16	37.7	3	< 20	1019	0.01	< 0.04	1.24
KSP2[b]	0.706856	0.000011	0.706842	63.83	Lamberti	163.16	37.7	4	25	1104	0.01	0.05	1.34
Strontium isotope data from Russian Platform													
RMn12	0.707177	0.000011	0.707170	108.10	Fulgens	146.76	37.5	4	< 20	1380	0.01	< 0.04	1.68
RMn10	0.707196	0.000009	0.707190	108.10	Fulgens	146.76	38.6	1	< 20	1514	0.00	< 0.04	1.79
RMn8	0.707198	0.000012	0.707191	108.10	Fulgens	146.76	38.8	< 1	< 20	1500	0.00	< 0.04	1.77
RT1b	0.706966	0.000010	0.706959	90.76	Lallieranum	153.85	38.7	2	< 20	1253	0.00	< 0.04	1.48
RT1a	0.706939	0.000013	0.706932	90.76	Lallieranum	153.85	38.7	2	< 20	1276	0.00	< 0.04	1.51
RT15	0.706939	0.000012	0.706932	90.32	Mutabilis	154.00	38.5	4	< 20	1269	0.01	< 0.04	1.51
RT24a	0.706944	0.000009	0.706938	90.14	Mutabilis	154.07	38.2	2	< 20	1102	0.00	< 0.04	1.32
RT16	0.706940	0.000014	0.706933	89.61	Mutabilis	154.26	38.3	1	< 20	1235	0.00	< 0.04	1.47
RT20	0.706934	0.000010	0.706927	88.28	Uhlandi	154.61	38.7	2	< 20	1143	0.00	< 0.04	1.35
RT4	0.706944	0.000008	0.706937	88.04	Uhlandi	154.65	39	2	< 20	1235	0.00	< 0.04	1.45
RT21	0.706930	0.000011	0.706923	87.96	Uhlandi	154.67	38.6	6	< 20	1144	0.01	< 0.04	1.36
RT8	0.706937	0.000008	0.706931	87.90	Uhlandi	154.68	38.1	9	< 20	1192	0.02	< 0.04	1.43
RMII43[d]	0.706891	0.000008	0.706885	82.49	Polygyratus	155.95	37.6	4	< 20	1160	0.01	< 0.04	1.41
RMI45[d]	0.706896	0.000009	0.706890	82.38	Polygyratus	155.97	38.1	7	< 20	1193	0.01	< 0.04	1.43
RMII41[d]	0.706896	0.000012	0.706889	82.33	Polygyratus	155.97	37.9	3	< 20	1221	0.01	< 0.04	1.47

(continued on next page)

Table 1 *(continued)*

Sample	$^{87}Sr/^{86}Sr$ measured	2 s.e.	$^{87}Sr/^{86}Sr$ normal.	Position	(Sub)zone	Age (Ma)	Ca (ppm)	Mn (ppm)	Fe (ppm)	Sr (ppm)	Mn/Ca * 1000	Fe/Ca * 1000	Sr/Ca * 1000
Strontium isotope data from northern Slovakia													
KAM30[e]	0.707191	0.000011	0.707184	19.79	Hebridica	169.72	40.0	41	146	1014	0.07	0.26	1.16
KAM14[e]	0.707185	0.000011	0.707179	19.01	Hebridica	169.79	39.4	35	146	1022	0.06	0.27	1.19
KAM1[e]	0.707275	0.000011	0.707268	19.01	Hebridica	169.79	38.4	15	121	1106	0.03	0.23	1.32
Strontium isotope data from Western Siberia (cf. Shurygin et al., 2015)													
MR54.9-10[f]	0.707267	0.000005	0.707240	115.50	Kochi	142.10	38.5	4	5	1370	0.01	0.01	1.63
MR54.8-05[f]	0.707253	0.000005	0.707226	114.47	Sibiricus	143.06	38.8	6	65	1290	0.01	0.12	1.52
MR54.7-25[f]	0.707258	0.000004	0.707231	114.37	Sibiricus	143.17	37.8	5	5	1340	0.01	0.01	1.62
MR54.7-05[f]	0.707246	0.000005	0.707219	114.16	Sibiricus	143.40	38.3	3	13	1240	0.01	0.02	1.48
MR54.6-85[f]	0.707247	0.000006	0.707220	113.88	Chetae	143.70	38.2	9	5	1340	0.02	0.01	1.60
MR54.6-50[f]	0.707227	0.000005	0.707200	113.60	Chetae	144.00	39.4	12	8	1300	0.02	0.01	1.51
MR54.6-30[f]	0.707233	0.000005	0.707206	113.44	Chetae	144.17	38.1	8	15	1090	0.02	0.03	1.31
MR54.6-25[f]	0.707228	0.000005	0.707201	113.40	Chetae	144.21	38.1	6	5	1160	0.01	0.01	1.39
MR54.6-00[f]	0.707242	0.000006	0.707215	113.20	Chetae	144.43	35.3	6	6	1150	0.01	0.01	1.49
MR54.5-95[f]	0.707243	0.000006	0.707216	113.16	Chetae	144.47	36	8	5	1120	0.02	0.01	1.42
MR54.5-85[f]	0.707237	0.000006	0.707210	113.08	Chetae	144.55	35.5	3	31	1100	0.01	0.06	1.42
MR54.5-70[f]	0.707229	0.000005	0.707202	112.92	Milkovensis	144.72	36.2	5	6	1350	0.01	0.01	1.71
MR54.5-60[f]	0.707224	0.000005	0.707197	112.78	Milkovensis	144.87	35.4	7	19	1370	0.01	0.04	1.77
MR54.5-50[f]	0.707229	0.000004	0.707202	112.64	Milkovensis	145.02	38.5	4	20	1120	0.01	0.04	1.33
MR54.5-45[f]	0.707222	0.000006	0.707195	112.58	Milkovensis	145.09	36.9	16	4	1240	0.03	0.01	1.54
MR54.5-30[f]	0.707218	0.000004	0.707191	112.36	Milkovensis	145.32	37.2	4	2	1440	0.01	0.00	1.77
MR54.5-20[f]	0.707220	0.000005	0.707193	112.22	Milkovensis	145.47	37.6	17	4	1320	0.03	0.01	1.61
MR54.5-00[f]	0.707214	0.000006	0.707187	111.92	Nodiger	145.72	37.3	2	5	1290	0.00	0.01	1.58
MR54.4-10[f]	0.707219	0.000005	0.707192	111.72	Nodiger	145.78	36.7	9	17	1280	0.02	0.03	1.60
MR54.3-105[f]	0.707218	0.000006	0.707191	111.14	Nodiger	145.95	38	4	5	1140	0.01	0.01	1.37
MR54.3-20[f]	0.707197	0.000006	0.707170	109.74 (± 1.5)	Subfulgens	146.40 (± 0.41)	39.1	2	5	1280	0.00	0.01	1.50
MR54.2-00[f]	0.707204	0.000005	0.707177	108.84 (± 1.5)	Fulgens	146.65 (± 0.34)	38.9	11	57	1210	0.02	0.11	1.42
MR54.1-20[f]	0.707203	0.000005	0.707176	108.33 (± 1.5)	Fulgens	146.73 (± 0.3)	37.9	29	8	1080	0.06	0.02	1.30

[a] Samples, whose elemental concentrations are reported after Wierzbowski (2004)
[b] Samples, whose elemental concentrations are reported after Wierzbowski (2015).
[c] Samples, whose elemental concentrations are reported after Wierzbowski et al. (2009).
[d] Samples, whose elemental concentrations are reported after Wierzbowski et al. (2013)
[e] Samples, whose elemental concentrations are reported after Arabas (2016).
[f] Samples, whose elemental concentrations are reported after Dzyuba et al. (2013).

System	Substage	Ammonite zone	Ammonite subzone	Base (stratigraphical scale)	Duration (Ma)	Base (Ma)
Cretaceous	Ryazanian (pars)	Tzikwinianus		117	0.78	140.94
		Rjasanensis	Transfigurabilis	116	0.77	141.71
			Kochi	115	0.77	142.48
		stratigraphic gap (=Sibiricus)		114	1.09	143.57
	Upper Volgian	Singularis (=Chetae)		113	1.07	144.64
		Nodiger	Milkovensis	112	1.06	145.70*
Jurassic			Nodiger	111	0.29	145.99
		Catenulatum (Subditus)		110	0.33	146.32
		Fulgens	Subfulgens (Nekrasovi)	109	0.30	146.62
			Fulgens	108	0.16	146.78
	Middle Volgian	Nikitini	Nikitini	107	0.15	146.93
			Lahuseni	106	0.16	147.09
			Bipliciformis	105	0.15	147.24
		Virgatus	Rosanovi (Ivanovi)	104	0.15	147.39
			Virgatus	103	0.16	147.55
			Gerassimovi	102	0.15	147.70
		Panderi	Zarajskensis	101	0.19	147.89
			Scythicus	100	0.22	148,11
	Lower Volgian	Pseudoscythica	Puschi (Tenuicostatum)	99	1,37	149.48
			Pseudoscythica	98	1.07	150.55
		Sokolovi		97	0.53	151.08
		Klimovi		96	0.98	152.06*
	Upper Kimmeridgian	Autissiodorensis	Fallax	95	0.38	152.44
			Subborealis	94	0.37	152.81
		Eudoxus	Contejani	93	0.32	153.13
			Caletanum	92	0.31	153.44
			Orthocera	91	0.32	153.76
		Mutabilis	Lallierianum	90	0.36	154.12
			Mutabilis	89	0.35	154.47*
	Lower Kimmeridgian	Divisum	Uhlandi	88	0.19	154.66
			Tenuicostata	87	0.18	154.84*
		Hypselocyclum	Lothari	86	0.38	155.22
			Hyppolytense	85	0.38	155.60*
		Platynota	Guilherandense	84	0.14	155.74
			Desmoides	83	0.14	155.88
			Polygyratus	82	0.14	156.02*
		Planula	Galar	81	0.37	156.39
			Planula	80	0.36	156.75*
		Bimammatum	Hauffianum	79	0.28	157.03
			Bimammatum	78	0.27	157.30*
	Upper Oxfordian	Hypselum		77	1.24	158.54*
		Bifurcatus	Grossouvrei	76	0.30	158.84
			Stenocycloides	75	0.30	159.14
			Wartae	74	0.30	159.44*
	Middle Oxfordian	Transversarium	Elisabethae	73	0.39	159.83
			Buckmani	72	0.38	160.21
		Plicatilis	Arkelli	71	0.21	160.42
			Ouatius	70	0.21	160.63
			Paturattensis	69	0.21	160.84*
	Lower Oxfordian	Cordatum	Cordatum	68	0.18	161.02
			Costicardia	67	0.19	161.21
			Bukowskii	66	0.18	161.39*
		Mariae	Praecordatum	65	0.86	162.25
			Scarburgense	64	0.85	163.10*
	Upper Callovian	Lamberti	Lamberti	63	0.36	163.46
			Henrici	62	0.35	163.81*
		Athleta	Spinosum	61	0.05	163.86
			Proniae	60	0.06	163.92
			Phaeinum	59	0.05	163.97*
	Middle Callovian	Coronatum	Grossouvrei	58	0.27	164.24
			Obductum	57	0.26	164.50*
		Jason	Jason	56	0.07	164.57
			Medea	55	0.06	164.63*
	Lower Callovian	Calloviense	Enodatum	54	0.19	164.82
			Calloviense	53	0.19	165.01
		Koenigi	Galilaei	52	0.20	165.21
			Curtilobus	51	0.19	165.40
			Gowerianus	50	0.19	165.59*
		Hervei	Kamptus	49	0.16	165.75
			Terebratus	48	0.16	165.91
			Keppleri	47	0.16	166.07*
	Upper Bathonian	Discus	Discus	46	0.09	166.16
			Hollandi	45	0.08	166.24*
		Retrocostatum	Histricoides	44	0.08	166.32
			Hodsoni	43	0.09	166.41
			Quercinus	42	0.08	166.49*
	Middle Bathonian	Bremeri	Fortecostatum	41	0.09	166.58
			Bullatimorphis	40	0.08	166.66*
		Morrisi		39	0.12	166.78*
		Subcontractus		38	0.13	166.91*
		Progracilis	Progracilis	37	0.23	167.14
			Orbini	36	0.23	167.37*
	Lower Bathonian	Tenuiplicatus		35	0.45	167.82*
		Zigzag	Yeovilensis	34	0.15	167.97
			Macrescens	33	0.13	168.10
			Convergens	32	0.18	168.28*
	Upper Bajocian	Parkinsoni	Bomfordi	31	0.14	168.42
			Parkinsoni	30	0.13	168.55
			Acris	29	0.14	168.69*
		Garantiana	Tetragona	28	0.14	168.83
			Subgaranti	27	0.14	168.97
			Dichotoma	26	0.14	169.11*
		Niortense	Baculata	25	0.11	169.22
			Polygyralis	24	0.12	169.34
			Banksi	23	0.11	169.45*
	Lower Bajocian	Humphriesianum	Blagdeni	22	0.08	169.53
			Humphriesianum	21	0.09	169.62
			Romani	20	0.08	169.70*
		Propinquans	Hebridica	19	0.09	169.79
			Patella	18	0.08	169.87*
		Laeviscula	Laeviscula	17	0.13	170.00
			Ovalis	16	0.13	170.13*
		Discites	Subsectum	15	0.09	170.22
			Walkeri	14	0.08	170.30*
	Upper Aalenian	Concavum	Limitatum (Formosum)	13	0.27	170.57
			Concavum	12	0.26	170.83*
	Middle Aalenian	Bradfordensis	Gigantea	11	0.23	171.06
			Bradfordensis	10	0.23	171.29*
		Murchisonae	Murchisonae	9	0.42	171.71
			Haugi	8	0.42	172.13*
	Lower Aalenian	Opalinum	Comptum (Scissum)	7	1.01	173.14
			Opalinum	6	1.01	174.15*
	Upper Toarcian (pars)	Aalensis	Fluitans	5	0.14	174.29
			Mactra	4	0.14	174.43*
		Pseudoradiosa	Pseudoradiosa	3	0.14	174.57
			Levesquei	2	0.14	174.71*
		Dispansum	Gruneri	1	0.13	174.84
			Insigne	0	0.13	174.97*

Fig. 1. Ammonite-based zonal and subzonal scheme of the uppermost Lower Jurassic–lowermost Cretaceous adopted for the construction of seawater strontium isotope curves. Applied ammonite divisions are as follows: (1) for the Upper Toarcian is used the standard North-Western Europe zonation (cf. Simms et al., 2004); (2) for the Aalenian–Lower Bajocian is used a modified version of the standard Mediterranean zonation presented by Sandoval et al. (2002); (3) for the Upper Bajocian–Bathonian is used the standard Mediterranean zonation as presented by Groupe Français d'Étude du Jurassique (1997), Rioult et al. (1997), and Matyja and Wierzbowski (2000a), (4) for the Callovian–Lower Oxfordian is used the standard (Sub)Boreal zonation (cf. Groupe Français d'Étude du Jurassique, 1997); (5) for the Middle–Upper Oxfordnian is used the Submediterranean zonation of the peri-Carpathian Poland presented by Głowniak (1997, 2000, 2002); (6) for the Lower Kimmeridgian is used the standard Submediterranean zonation (cf. Groupe Français d'Étude du Jurassique, 1997); (7) and for the Upper Kimmeridgian–Ryazanian is employed the Boreal zonation of the Russian Platform (cf. Rogov, 2004, 2010a, 2014; Schnabl et al., 2015; Shurygin and Dzyuba, 2015; Rogov et al., 2015b). For precise correlations between regional ammonite zonal schemes see text and Figs. 2–5. The biostratigraphical scale is based on the assumed equal duration of ammonites subchrons, which are counted successively starting from the base of the studied interval. The numerical time scale is based on published radiometric and cyclostratigraphical data (marked with asterisks; after Ogg et al., 2012, 2016). The published chronological data have been interpolated into the subchron level assuming equal duration of each subchron, and if necessary re-adjusted to the correlation between various ammonite zonal schemes (see Figs. 2–5).

Strontium was extracted on an ion-exchange resin Dowex AG50Wx8 (200–400 mesh) using 2.5 N HCl as eluent. Strontium isotopic composition was measured on the multicollector thermal ionization mass spectrometer Triton TI in a static collection mode using rhenium filament ion source. Reproducibility of $^{87}Sr/^{86}Sr$ ratios of NIST SRM 987 and USGS EN-1 standards, normalized to $^{86}Sr/^{88}Sr = 0.1194$, was 0.710275 ± 0.000008 (2SD, n = 36) and 0.709202 ± 0.000006 (2SD, n = 16), respectively. Data normalization procedures were the same as described above.

The biostratigraphical scale of the diagrams is based on the assumed equal duration of ammonites subchrons, which are counted successively starting from the base of the studied interval, i.e. the Insigne Subzone of the Dispansum Zone of the uppermost Toarcian (Fig. 1). A few non-subdivided chrons are assumed to be equal to single subchrons. The time scale of the chronological diagram is based on published, numerical ages determined using radiometric methods and cyclostratigraphical scaling of ammonite chrons (after Ogg et al., 2012, 2016). The published chronological data have been interpolated into the subchron level (assuming equal duration of each subchron), and if necessary re-adjusted to the correlation between different ammonite zonal schemes (see Figs. 2–5).

The strontium isotope curve was estimated using the locally weighted scatterplot smoothing (LOWESS) regression model (cf. Cleveland, 1979). Results of LOWESS regression depend on chosen smoothing parameter (span). The span parameter is defined as a fraction of the total number of data points (n) used for the calculation of the model value at a given point. An appropriate span value is chosen using trade-off between goodness-of-fit at local, and global scales (cf. Howarth and McArthur, 1997). The chosen span value allows estimation of the less smoothed model which is robust against bias coming from outliers. Two variables i.e. age and $^{87}Sr/^{86}Sr$ ratio need to be taken into account by the estimation of a reliable LOWESS model (Hercman, 2009). MOD-AGE algorithm based on the Monte Carlo method is used to solve this problem (cf. Hercman and Pawlak, 2012). The MOD-AGE algorithm has allowed us to estimate 95% confidence intervals for data series. Owing to the fact that uncertainties of measurements of $^{87}Sr/^{86}Sr$ ratios are almost constant confidence limits of marine $^{87}Sr/^{86}Sr$ curve reflect uncertainties of stratigraphical and numerical dating of samples and density of data points.

4. Temporal trends and stratigraphical correlations

The samples, whose $^{87}Sr/^{86}Sr$ ratios are used for the construction of isotope curve, are dated according the biostratigraphical zonal schemes specific for their area of origin (cf. Jones et al., 1994a, 1994b; Schweigert and Callomon, 1997; Callomon and Dietl, 2000; McArthur et al., 2000; Jenkyns et al., 2002; Wierzbowski, 2002, 2004, 2015; Gröcke et al., 2003; Page et al., 2009; Głowniak et al., 2010; Segit,

Substage	Poland (this study) Zone	Subzone	Position of the base	Switzerland Zone	Subzone	Position of the base	SE France & Spain Zone	Subzone	Position of the base
Low. Kim.	Bimammatum	Bimammatum	78	Bimammatum	Bimammatum	78	Bimammatum	Bimammatum	78
Upper Oxfordian	Hypselum		77		Hypselum	77		Hypselum	77
	Bifurcatus	Grossouvrei	76	Bifurcatus	Grossouvrei	76	Bifurcatus	Grossouvrei	76
		Stenocycloides	75		Stenocycloides	75		Stenocycloides	75
		Wartae	74	Schilli	Rotoides	74.39	Transversarium	Rotoides	74.39
					Schilli	73.88		Schilli	~73.88
Middle Oxfordian	Transversarium	Elisabethae	73	Transversarium	Luciaeformis	73.13		Luciaeformis	74.13
		Buckmani	72		Antecedens	71.90		Parandieri	72.46
	Plicatilis	Arkelli	71		Densiplicatum	69	Plicatilis	Antecedens	~71
		Ouatius	70					Vertebrale	69
		Patturatensis	69						
L.O.	Cordatum	Cordatum	68	Cordatum	Cordatum	68	Cordatum	Cordatum	68

Fig. 2. Correlation between Submediterranean ammonite zonal schemes of the Middle–Upper Oxfordian of Europe (after Głowniak, 2006; modified). Position of the base of each stratigraphical division is given in subchron unit scale according to Fig. 1. L.O. – Lower Oxfordian.

2010; Wierzbowski et al., 2012, 2013; Rogov, 2014; Rogov and Starodubtseva, 2014; Arabas, 2016).

Although the uppermost Toarcian–Lower Kimmeridgian ammonite zonation used in the present study (see Fig. 1) is transregional and preferred for European parts of the (*peri*)-Tethyan and Subboreal provinces some differences exist in terms of the duration of the

Peri-Carpathian Poland (Submediterranean Province; this study) Substage	Zone	Subzone	Position of the base	Russian Platform (Subboreal Province) Substage	Zone	Subzone	Position of the base
Lower Kimmeridgian	Platynota	Guilherandense	84	Lower Kimmeridgian	Kitchini	Modestum	83
		Desmoides	83				
		Polygyratus	82			Subkitchini	81
	Planula	Galar	81				
		Planula	80		Bauhini		78
	Bimammatum	Hauffianum	79				
		Bimammatum	78				
Upper Oxfordian	Hypselum		77	Upper Oxfordian	Rosenkrantzi		77
	Bifurcatus	Grossouvrei	76		Regulare		76.10
						Serratum	75.73
		Stenocycloides	75		Serratum	Koldeweyense	75.33
		Wartae	74		Glosense	Glosense	73.94
Middle Oxfordian	Transversarium	Elisabethae	73			Ilovaiskii	73.44
		Buckmani	72	Middle Oxfordian	Tenuiserratum	Blakei	72.75
						Tenuiserratum	72.50
						Maltonense	71.50
	Plicatilis	Arkelli	71		Densiplicatum	Vertebrale	69
		Ouatius	70				
		Patturatensis	69				
Lower Oxfordian	Cordatum	Cordatum	68	Lower Oxfordian	Cordatum	Cordatum	68
		Costicardia	67			Costicardia	67
		Bukowskii	66			Bukowskii	66
	Mariae	Praecordatum	65		Mariae	Praecordatum	65
		Scarburgense	64			Scarburgense	64
Upper Callovian	Lamberti	Lamberti	63	Upper Callovian	Lamberti	Lamberti	63
		Henrici	62			Henrici	62
	Athleta	Spinosum	61		Athleta	Spinosum	61
		Proniae	60			Proniae	60
		Phaeinum	59			Phaeinum	59

Fig. 3. Correlation between Submediterranean and Boreal ammonite zonal schemes of the uppermost Callovian–lowermost Kimmeridgian of the peri-Carpathian Poland and the Russian Platform (after Głowniak et al., 2010; and Wierzbowski et al., 2013; modified). Position of the base of each stratigraphical division is given in subchron unit scale according to Fig. 1.

Central Poland, S Germany, SE France (Submediterranean Province)				Russian Platform (Subboreal Province)		
Substage	Zone	Subzone	Position of the base	Zone	Subzone	Position of the base
Upper Kimmeridgian (pars)	Beckeri (pars)		92.70	Eudoxus	Contejani	93
					Caletanum	92
	Pseudomutabilis		90.80		Orthocera	91
	Acanthicum		89	Mutabilis	Lallieranum	90
					Mutabilis	89
Lower Kimmeridgian (pars)	Divisum	Uhlandi	88		Askepta	86.78
		Tenuicostata	87			
	Hypselocyclum	Lothari	86	Cymodoce (pars)	Cymodoce (pars)	
		Hyppolytense	85			

Fig. 4. Correlation between Submediterranean and Subboreal ammonite zonal schemes of the Lower–Upper Kimmeridgian of Europe and the Russian Platform (after Matyja and Wierzbowski, 2000b and Scherzinger et al., 2016). Position of the base of each stratigraphical division is given in subchron unit scale according to Fig. 1.

Middle–Upper Oxfordian ammonite zones recognized in different areas. The Submediterranean Middle–Upper Oxfordian zonation currently employed is after Głowniak (1997, 2000, 2002), and based on the detailed study of perisphinctid ammonite fauna from the peri-Carpathian Poland. Its detailed correlation with the Western European Submediterranean zonal schemes has, recently, been presented (see Głowniak, 2006; and Fig. 2).

It is important to note that significant differences exist between the Submediterranean stratigraphical divisions of the Middle–Upper Oxfordian and the Lower Kimmeridgian and the (Sub)Boreal ammonite

Russian Platform (this study): Sub-stage	Zone	(Sub)Zone	Position of the base
UPPER VOLGIAN	Singularis	Singularis	113
	Nodiger	Milkovensis	112
		Nodiger	111
	Catenulatum	Catenulatum	110
	Fulgens	Subfulgens	109
		Fulgens	108
MIDDLE VOLGIAN	Nikitini	Nikitini	107
		Lahuseni	106
		Bipliciformis	105
	Virgatus	Rosanovi	104
		Virgatus	103
		Gerassimovi	102
	Panderi	Zarajskensis	101
		Scythicus	100
LOWER VOLGIAN	Pseudo-scythica	Puschi	99
		Pseudoscythica	98
	Sokolovi	Sokolovi	97
	Klimovi	Klimovi	96

Northern Siberia: Zone	(Sub)Zone	Position of the base
Chetae	Chetae	113
Taimyrensis	Taimyrensis	112
		111
Okensis	Originalis	110
	Okensis	108
Exoticus	Exoticus	107.13
Variabilis	Variabilis	105.25
Excentricus	Excentricus	103.87
Maximus	Maximus	102
Ilovaiskii	Ilovaiskii	101.22
Iatriensis	Iatriensis	100
Pectinatus	Pectinatus	~98.58
Subcrassum	Subcrassum	~96.70
Magnum	Magnum	96

East Greenland: Zone	Position of the base
Chetaites chetae beds	~113
? Subcraspedites sowerbyi beds	~108
Praechetaites tenuicostatus beds	107.13
Vogulicus	105.94
Groenlandicus	105.25
Anguinus	103.87
Pseudapertum	102
Gracilis	101.58
Liostracus	101.22
Communis	100.91
Rugosa	100.64
Iatriensis	100.29
Primus	100
Pectinatus	98.39
Hudlestoni	97.87
Wheatleyensis	97.29
	96.61
Elegans	96

England, N. France, North Sea: Stage	Zone	Position of the base
PORTLANDIAN	Lamplughi	113
	Preplicomphalus	~107.73
	Primitivus	~107.25
	? Oppressus	~106.42
	Anguiformis	105.82
	Kerberus	105.30
	Okusensis	104.42
	Glaucolithus	102.81
	Albani	102
BOLONIAN	Fittoni	101.19
	Rotunda	100.67
	Pallasioides	100.06
	Pectinatus	98.39
	Hudlestoni	97.88
	Wheatleyensis	97.29
	Scitulus	96.61
	Elegans	96

SW Germany, N Italy, Spain: Sub-stage	Zone	(Sub)Zone	Position of the base
LOWER BERRIASIAN	Jacobi	Grandis	~113
		Jacobi	112
UPPER TITHONIAN			~111.13
		Durangites	~109.11
		Microcanthum	101.86
LOWER TITHONIAN		Palmatus (= Ponti)	100.02
		Ciliata (= Fallauxi + Semiforme)	98.32
	Dar-wini	Vimineus	97.62
		Mucronatum	97.14
	Hybo-notum	Moernsheimensis	96.56
		Rupelianum	96.33
		Riedense	96

Position of J-K boundary defined as the base of the calpionellid Alpina Zone

Fig. 5. Correlation of the Volgian zonal scheme of the Russian Platform with biostratigraphical subdivisions of other areas of the Boreal province, the Bolonian–Portlandian of England, N France, and North Sea as well as the Tithonian–Early Berriasian of SW Germany, N Italy and Spain (after Zeiss, 2003; Rogov and Zakharov, 2009; Rogov, 2014; Vašiček and Skupien, 2014; Shurygin and Dzyuba, 2015; Pszczółkowski, 2016). Position of the base of each stratigraphical division is given in subchron unit scale according to Fig. 1.

zonal scheme, based on cardioceratid ammonites. Because of the differences the boundary of the Oxfordian and the Kimmeridgian stages was placed in different chronostratigraphic equivalents in the (Sub) Boreal and Submediterranean bioprovinces (cf. Matyja and Wierzbowski, 1995). A new recommendation of the Kimmeridgian Working Group of the International Subcomission on Jurassic Stratigraphy is to use in the (Sub)Boreal definition of the Oxfordian–Kimmeridgian boundary, which is an equivalent of the boundary between the Submediterranean Hypselum and Bimammatum zones (cf. Ogg et al., 2012; Wierzbowski and Matyja, 2014; Wierzbowski et al., 2016). Precise correlation of the Boreal ammonite zonal scheme of the Oxfordian and the Lower Kimmeridgian of the Russian Platform with the Submediterranean zonation of the peri-Carpathian Poland is given on Fig. 3 to clarify any doubts concerning dating of strontium isotope variations in this interval.

The most important differences exist, however, in the stratigraphical zonal schemes of the latest Jurassic and the earliest Cretaceous (Upper Kimmeridgian–Beriassian). They result from significant provincialism of ammonite faunas in this period. The (Sub) Boreal Upper Kimmeridgian–Ryazanian ammonite zonation of the Russian Platform is employed in the current study owing to the area of origin of the majority of the strontium isotope data (cf. Gröcke et al., 2003; Rogov and Starodubtseva, 2014; Rogov et al., 2014, Rogov et al., 2015b; see also Fig. 1).

Subboreal Upper Kimmeridgian zonal scheme of the Russian Platform is similar to the British ammonite zonation, and the same subzones as in NW Europe are applied for the subdivision of the Mutabilis and Eudoxus zones in this area. The Autisiodерensis and the Irius subzones of the Autissiodorensis Zone in the NW Europe are, however, not clearly defined. Accepting the First Appearance Datum (FAD) of *Gravesia*, which is nearly coincides with the FAD of *Aulacostephanus mammatus*, as a marker for the base of the NW Europe Irius Subzone (= Mammatus Subzone sensu Van der Vyver, 1986), it is necessary to place this boundary slightly below the boundary between the Subborealis and Fallax subzones of the Autissiodorensis Zone in the Russian Platform (cf. Rogov, 2010a). Correlation between the Submediterranean and the Subboreal ammonite zonal schemes of the Lower–Upper Kimmeridgian, as presented by Matyja and Wierzbowski (2000b), and Scherzinger et al. (2016), is given on Fig. 4.

Kimmeridgian–Volgian and Kimmeridgian-Tithonian boundaries are coincident, and well-marked by the total disappearance of aulacostephanids, in both the Mediterranean and the Boreal bioprovinces (cf. Rogov, 2011, 2014; Gallois, 2011, 2012). An additional evidence for the correlation of the base of the Volgian Stage with that of the Tithonian is the similarity of *Neochetoceras* ammonite succession in both bioprovinces (Rogov, 2010a; Fig. 5).

Correlation of the Lower Volgian succession with the Tithonian one is possible based on occurrences of ammonites of Submediterranean affinities in the Lower Volgian of the Polish Lowland (Kutek and Zeiss, 1997) and the Volga area (Rogov, 2004, 2010a, 2014). However, above the neoburgense horizon of the Lower Volgian Pseudoscythica Zone, only rare ammonites of Submediterranean origin occur in the Russian Platform (mainly *Haploceras* sp., see Rogov, 2013, 2014), and above the Middle Volgian Panderi (= Scythicus) Zone these ammonites totally disappear. The correlation of the Lower and the Upper Tithonian boundary with the Boreal ammonite zonal scheme has been, however, recently documented by the occurrence of chitonoidellids of the lowermost Upper Tithonian in the uppermost part of the Panderi Zone in central Poland (cf. Lakova and Petrova, 2013; Matyja and Wierzbowski, 2016; Pszczółkowski, 2016).

Correlation of the majority of the Middle and the Upper Volgian ammonite zonal boundaries with the Tithonian and the Berriassian ones remains tentative. It is principally based on palaeomagnetic data, mainly from the Nordvik section (Northern Siberia; Houša et al., 2007; Bragin et al., 2013, Rogov, 2014; Schnabl et al., 2015; Shurygin and Dzyuba, 2015), and only some correlations based on ammonite successions of the Northern Siberia and the Russian Platform are possible (Rogov, 2010b). It is important to note that a recently proposed position of the Tithonian–Berriassian boundary (by the Berriasian Working Group of the International Subcomission on Jurassic Stratigraphy), is defined on the basis of calpionellid fauna, and lies at the base of the calpionellid Alpina Zone. Its time equivalent in the J-K Boreal auxiliary stratotype – the Nordvik section is devoid of ammonites (Rogov et al., 2015a). Preliminary palaeomagnetic data derived from highly condensed Kashpir section (Middle Volga area) suggest that at such definition the base of the Berriasian lies within the Boreal Nodiger ammonite zone (Baraboshkin et al., 2016), whose lower boundary is coincident with that of the Taimyrensis Zone of the Northern Siberia. Recent state of knowledge on the correlation of the Volgian ammonite zonal scheme of the Russian Platform with biostratigraphical subdivisions of other areas of the Boreal province, the Bolonian–Portlandian of NW Europe and the Tithonian–Early Berriasian of SW Germany, N Italy, and Spain, as based on studies of Zeiss (2003), Rogov and Zakharov (2009), Rogov (2014), Vašiček and Skupien (2014), Shurygin and Dzyuba (2015), and Pszczółkowski (2016) is presented on Fig. 5.

The correlation of the Ryazanian ammonite zonation of the Russian Platform with that of the Northern Siberia and the Berriasian one is also unclear and based on ammonite and palaeomagnetic data (cf. Baraboshkin, 1999; Mitta, 2005, 2007; Shurygin and Dzyuba, 2015; Rogov et al., 2017). We follow, for the studied parts of the Ryazanian, known information on the correlation between Russian Platform and Northern Siberia ammonite zones (cf. Rogov et al., 2015b), and recent correlations between the Boreal-Siberian and the Mediterranean ammonite zonal schemes presented in Shurygin and Dzyuba (2015) and Rogov et al. (2017).

Another important question concerns a need of re-positioning of some published strontium isotope data from the Russian Platform in the stratigraphical chart as based on the improved stratigraphical dating of some parts of the sections studied previously. The dating of some samples of Podlaha et al. (1998) and Gröcke et al. (2003) derived from the sections: Gorodishchi (= "Gorodische"), Kashpir, Peski, Rybinsk – Ioda river (= "Jaroslawskaja") has been revised according to the new stratigraphical data of Smirnova et al. (1999), Kiselev (2003), Vishnevskaya and Baraboshkin (2001), Bragin and Kiselev (2013), Rogov et al. (2015b; see also: Głowniak et al., 2010; Wierzbowski et al., 2013).

5. Diagenetical alteration

Strontium isotope composition of marine carbonates is susceptible to the alteration in burial and meteoric environments. Diagenetic alteration often results in simultaneous variations in isotope ratios, and elemental concentrations in calcite (cf. Veizer, 1983; Banner and Hanson, 1990; Banner, 1995). Marine shells are characterized by certain Mn, Fe, and Sr concentrations; measurements of concentrations of these elements in fossils allow, therefore, screening for their preservation state (Veizer, 1974, 1983; Brand and Veizer, 1980; Marshall, 1992; Ullmann and Korte, 2015). Mn^{2+} ions are an activator of orange-red cathodoluminescence in calcites, which is indicative of the alteration under reducing conditions (Marshall, 1992; Savard et al., 1995).

Non-luminescent parts of newly collected belemnite rostra have only been sampled (Fig. 6). Accepted limits of Mn, Fe, and Sr concentrations in well-preserved Jurassic carbonate fossils differ depending on sedimentary settings and opinions of researchers (cf. Veizer, 1974; Jones et al., 1994a; Nunn et al., 2009; Alberti et al., 2012; Wierzbowski, 2013, 2015; Ullmann and Korte, 2015). To be in line with previous studies of Jones et al. (1994a, 1994b) and Wierzbowski et al. (2012) we follow, in the present contribution, accepted upper limits of Mn (50 ppm) and Fe (150 ppm) in well-preserved belemnite rostra and oyster shells. Lower limits of Sr concentration (800 ppm) in belemnite rostra have been accepted in agreement with the suggested concentration of strontium in well-preserved material from the Russian

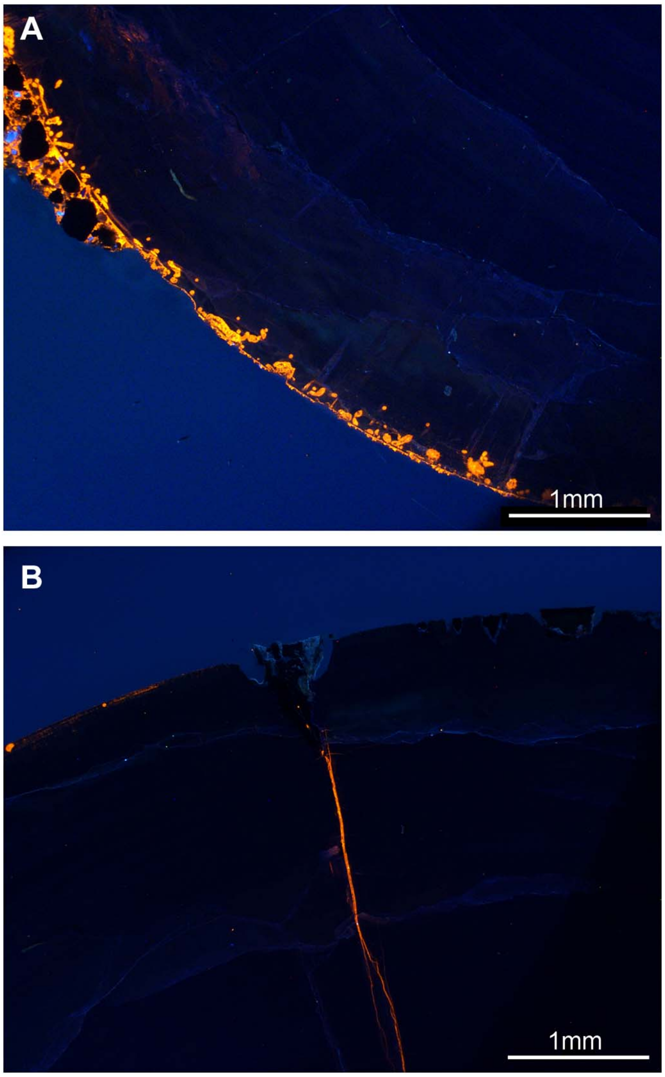

Fig. 6. Cathodoluminescence images of newly collected belemnite rostra from the Tarkhanovskaya Pristan' section, Tatarstan, Russian Platform (Divisum Zone, Lower Kimmeridgian). A. Non-luminescent belemnite rostrum with drilled, and partially luminescent rim. Sample RT21. B. Non-luminescent belemnite rostrum with luminescent infilling of the alveolar fissure. Sample RT4.

Platform (cf. Wierzbowski et al., 2013). The accepted elemental concentrations in pure calcites are equivalents of Mn/Ca, Fe/Ca and Sr/Ca ratios of 0.09, 0.27 and 0.91 mmol/mol, respectively. Elemental ratios have been calculated for belemnite samples studied (Table 1). The given above thresholds of elemental ratios, or concentrations (if Ca content is not given) have been also applied for the selection of well-preserved samples from the datasets published previously. Unfortunately, not all the given criteria may be applied for some published datasets due a lack of information on some elemental concentrations. The preservation state of such samples is determined on the basis on available chemical proxies. An exception is also well-preserved belemnite material of McArthur et al. (2000), whose elevated Fe concentrations are linked the disseminated pyrite or iron oxides.

$^{87}Sr/^{86}Sr$ ratios of samples considered as diagenetically altered tend to plot above adjacent data points, although this is not a strict rule (Fig. 7). Higher $^{87}Sr/^{86}Sr$ ratios of diagenetically altered samples probably results from the post-depositional equilibration with diagenetic fluids enriched in radiogenic strontium (cf. Veizer, 1983; Banner and Hanson, 1990; Jones et al., 1994a, 1994b; Banner, 1995). This confirms the necessity of the elimination of diagenetically altered values from the strontium isotope dataset used for the construction of the Middle–Late Jurassic seawater curve.

6. Results

Seventy three new strontium isotope measurements (Table 1; cf. Wierzbowski et al., 2014; Shurygin et al., 2015) along with two hundred thirty seven published results of Jones et al. (1994a, 1994b), Callomon and Dietl (2000), McArthur et al. (2000), Jenkyns et al. (2002), Gröcke et al. (2003), McArthur et al. (2007), Page et al. (2009), Wierzbowski et al. (2012), which are derived from well-preserved and stratigraphically well-dated belemnite rostra and oyster shells, have been used for the determination of changes in seawater $^{87}Sr/^{86}Sr$ ratio during the Middle and the Late Jurassic (Fig. 7). The strontium isotope data of Podlaha et al. (1998), and the data of Vollstaedt et al. (2014), which are characterized by significant scatters, probably due to inaccurate dating, have been eliminated from this dataset. The same applies for data points from the "Oxfordian" subset of New Zealand samples of Gröcke et al. (2003), which are located distinctly below other coeval strontium data points. Most of New Zealand samples of Gröcke et al. (2003) are dated tentatively, and seem to be not suitable for the construction of temporal trends of variations in seawater strontium isotope ratio (Fig. 7).

The non-parametric LOWESS statistical functions based on the biostratigraphical and the numerical age time scales show variations of seawater $^{87}Sr/^{86}Sr$ ratio during the Middle–Late Jurassic (Figs. 8, 9). The seawater $^{87}Sr/^{86}Sr$ ratio was close to 0.70730 at the Toarcian–Aalenian transition, and throughout the Early Aalenian. It decreased a little starting from the Middle Aalenian, and reached a value of ca. 0.70729 at the Aalenian–Bajocian transition (Fig. 8). A rapid decrease of the seawater $^{87}Sr/^{86}Sr$ ratio is observed during the Bajocian. The ratio reached a value of ca. 0.70715 at the Early–Late Bajocian transition, and a value of ca. 0.70705 at the Bajocian–Bathonian transition. The seawater $^{87}Sr/^{86}Sr$ ratio still decreased in the course of the Bathonian, and the Early–Middle Callovian, reaching values of ca. 0.70704 at the Early–Middle Bathonian transition, ca. 0.70701 at the Middle–Late Bathonian transition, ca. 0.70695 at the Bathonian–Callovian transition, ca. 0.70687 at the Early–Middle Callovian transition, and ca. 0.70685 at the Middle–Late Callovian, and during the Late Callovian (Fig. 8). The lowest $^{87}Sr/^{86}Sr$ ratio of seawater is noted at the Early–Middle Oxfordian transition (ca. 0.70683). It was a turning point of the seawater strontium isotope curve and the ratio gradually increased during the rest of the Late Jurassic. The strontium isotope ratio of seawater reached the value of ca. 0.70687 at the Oxfordian–Kimmeridgian transition, according to the currently redefined biostratigraphical position of this boundary. A gradual increase of the ratio is observed during the Early Kimmeridgian and a more rapid increase starting from the Late Kimmeridgian. The ratio reached values of ca. 0.70694 at Early–Late Kimmeridgian transition, ca. 0.70705 at the Kimmeridgian–Volgian (= Kimmeridgian–Tithonian) transition, ca. 0.70711 at the Early–Middle Volgian transition, and ca. 0.70717 at the Middle–Late Volgian transition (ca. 0.70712 at the Early–Late Tithonian transition). During the Nodiger Chron of the Boreal Late Volgian, where is placed the Jurassic–Cretaceous transition defined according to the calpionellid zonal scheme, the $^{87}Sr/^{86}Sr$ seawater ratio was close to 0.70720 and increased further during the latest Volgian–Ryazanian (= Berriasian; Fig. 8).

The diagram based on the numerical time scale reveals non-symmetrical character of the Middle–Late Jurassic trough of the curve of the seawater $^{87}Sr/^{86}Sr$ ratio (Fig. 9). The ratio decreased relatively fast from ca. 0.70730 to ca. 0.70683, during the Middle Aalenian–Early Oxfordian, since 172.1 to 160.8 Ma ago (i.e. for 11.3 Ma). The non-complete recovery of the ratio during the Middle Oxfordian–Ryazanian (= Middle Oxfordian–Berriasian), to a value of ca. 0.70725, lasted, however, since 160.8 Ma to 140.9 Ma, i.e. its duration was 19.9 Ma. The seawater strontium isotope curve based on absolute time scale (Fig. 9) is similar to the LOWESS fit of the curve presented by McArthur

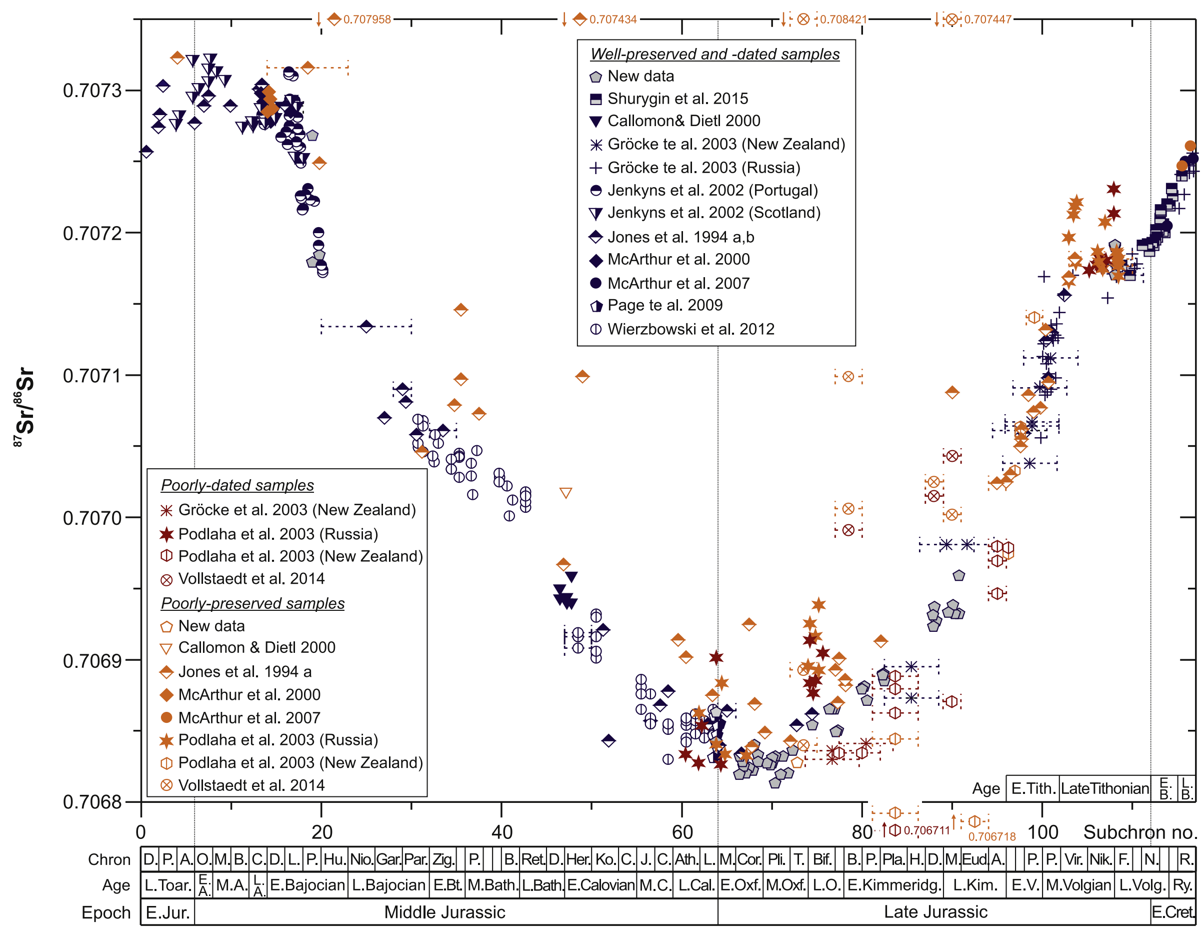

Fig. 7. Available strontium isotope data from the uppermost Lower Jurassic–lowermost Cretaceous. Well-preserved and well-dated samples – blue symbols; poorly-dated samples – dark red symbols; poorly-preserved samples – orange symbols. Data points derived from poorly-preserved samples tend to plot above general strontium isotope trend. The horizontal scale of the diagram is based on the biostratigraphical zonal scheme (see Fig. 1). Dating errors higher than one subchron are marked.

et al. (2012), which is based on GTS2012 time scale. Slight differences exist, however, between both curves. According to the new fit of the curve higher seawater $^{87}Sr/^{86}Sr$ ratios, than those predicted by McArthur et al. (2012), occurred during the Early–Middle Aalenian, and at the Jurassic–Cretaceous transition. Lower $^{87}Sr/^{86}Sr$ ratios are, in turn, determined for the Oxfordian–earliest Middle Volgian (= Oxfordian–Early Tithonian) interval (Fig. 9). The mean 95% confidence limits (2σ) of the current seawater $^{87}Sr/^{86}Sr$ curves are close to ± 0.000007 (Fig. 10), and take into account dating precision of some data points, which is of particular importance for relatively purely studied intervals. For such intervals, i.e. the Early–Late Bajocian transition, and the Early–Middle Volgian (= Early Tithonian–earliest Late Tithonian) the confidence limits of the curve are higher (up to ± 0.000035, or ± 0.000039 for stratigraphical scale and numerical age curve, respectively; Fig. 10), and higher than the confidence limits of the curve presented by McArthur et al. (2012; see Fig. 9).

7. Discussion

7.1. Revised Middle–Late Jurassic $^{87}Sr/^{86}Sr$ curve

The revised curve allows precise dating of variations of seawater $^{87}Sr/^{86}Sr$ ratio during the latest Early Jurassic–earliest Cretaceous. The verification of previously poorly known changes of seawater $^{87}Sr/^{86}Sr$ ratio during the Late Jurassic is essential for the chemostratigraphical use of the data (Figs. 7–9). This has been done by employment of strict criteria for the selection of reliable data points derived from published datasets, and by new measurements of strontium isotope ratios of numerous, well-preserved, and well-dated samples from the Oxfordian–Kimmeridgian and Jurassic–Cretaceous boundary interval.

The use of the regional (Tethyan to Boreal) biostratigraphical zonal schemes specific for the area of sample origin has enabled strict positioning of data points. The use of both biostratigraphical and numerical age scales have allowed precise dating of variations in the seawater $^{87}Sr/^{86}Sr$ ratio (Figs. 8, 9). Construction of the time-independent stratigraphical strontium isotope diagram is also important for the reduction of dating errors related to gradual modifications of the published numerical time frames of the Jurassic (cf. Gradstein et al., 2004; Gradstein, 2012; Ogg et al., 2012, 2016).

Thanks to the attached datasets (Tables S1 and S2) and the correlation tables (Figs. 1–5), any geological samples can be dated precisely, based on measured $^{87}Sr/^{86}Sr$ ratios, to the regional biostratigraphical framework i.e. particular zones and subzones of the uppermost Lower Jurassic–lowermost Cretaceous or to numerical ages. The current data impose re-definition of some published strontium isotope dating, e.g. the Oxfordian samples from the Cabaços, the lower part of the Cabo Mondego, and the upper part of the Cabo Mondego formations of central Portugal, dated previously, based on $^{87}Sr/^{86}Sr$ ratios, to the Bimammatum–Platynota zones, Plicatilis Zone, and the Bimammatum–Hypselocyclum zone, respectively (cf. Schneider et al., 2009) should be re-dated to the Planula–Platynota, Cordatum–Plicatilis, and the Bifurcatus–Hypselocyclum zones. This is due to a slightly different shape of the currently presented strontium isotope curve, compared to that of McArthur et al. (2001, 2012), and different position of the turning point of the Jurassic strontium isotope minimum.

Although the seawater $^{87}Sr/^{86}Sr$ ratio curve presented by McArthur

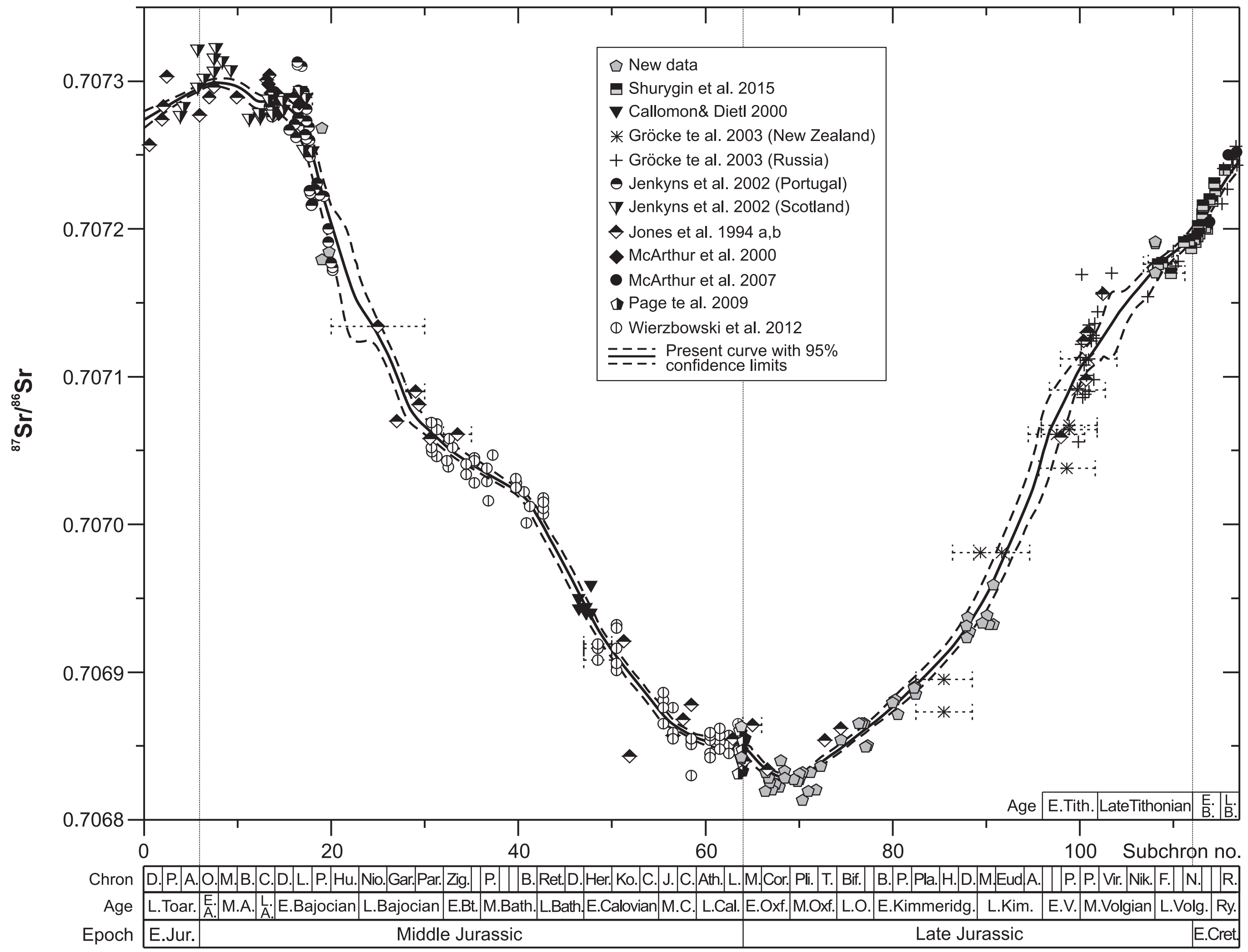

Fig. 8. Strontium isotope variations in the latest Early Jurassic–earliest Cretaceous. The Lowess curve (solid line), with given 95% confidence limits (dashed lines) is fitted to strontium isotope dataset of well-preserved fossils. The horizontal scale of the diagram is based on the biochronostratigraphical zonal scheme (see Fig. 1). Dating errors higher than one subchron are marked.

et al. (2012) has in many intervals lower width of confidence limits, than the new one, it seems to be an artefact owing to the underestimation of dating errors of data points used for the construction of the McArthur et al.'s curve (cf. Figs. 9, 10). Therefore, the width of 95% confidence limits (2σ) of the newly presented curve is considered to show realistic uncertainties in the estimation of Middle–Late Jurassic strontium isotope trends. Similar differences between a new fit of strontium isotope curve for the Permian and the curve presented by McArthur et al. (2012) have recently been shown by Korte and Ullmann (in press). This may only emphasise a role of numerous and well-positioned data points for the precise construction of the seawater $^{87}Sr/^{86}Sr$ curve.

7.2. Cause of variation of seawater $^{87}Sr/^{86}Sr$ ratio during the Middle–Late Jurassic

Continental weathering rates are often considered to have had a minor effect on the seawater strontium isotope pool during the Jurassic–Cretaceous (Jones and Jenkyns, 2001). Mesozoic seawater $^{87}Sr/^{86}Sr$ ratios are also postulated to be directly related to variations in subduction zone length (van der Meer et al., 2014). In addition, simultaneous changes in seawater $^{87}Sr/^{86}Sr$ and Sr/Ca ratios during the Early–Middle Jurassic point to predominant oceanic fluxes of strontium in this period (Ullmann et al., 2013). A Middle–earliest Late Jurassic fall in marine $^{87}Sr/^{86}Sr$ ratio is, therefore, interpreted as a result of the increased input of non-radiogenic, hydrothermal strontium to the seawater (Jones et al., 1994a; Wierzbowski et al., 2012). The $^{87}Sr/^{86}Sr$ ratio fall, which started at the Early–Middle Aalenian transition (172.1 Ma ago), despite the presence of a relatively low ratio of ca. 0.70730, and lasted till the Early–Middle Oxfordian transition (160.8 Ma ago) i.e. until a Phanerozoic seawater $^{87}Sr/^{86}Sr$ minimum of ca. 0.70683, is unusual. Although its magnitude ($^{87}Sr/^{86}Sr$ ratio change of 0.00047) is not the greatest, it is the steepest fall of the seawater strontium isotope ratio during the Phanerozoic (cf. McArthur et al., 2012), with the noted highest rates of change, of 0.00015, and 0.00009 per 1 Ma, during the mid-Bajocian (170.0 Ma ago), and at the Bathonian–Callovian transition (166. 1 Ma ago; Fig. 11), respectively. The enhanced hydrothermal strontium input to Middle Jurassic seawater was likely a consequence of the rapid acceleration of the volcanic activity of the oceanic crust. It may have been associated with the onset of seafloor spreading in the central Atlantic and the western Tethys, as well as the final breakup of Gondwana. All the processes are well-recognized, and dated mostly to the Bajocian–Callovian, based on ophiolites, and their sedimentary cover, rhyolitic magmas, stratigraphic sequence analyses, and palaeomagnetic studies (cf. Gradstein et al., 1991; Brassier and Geleta, 1993; Féraud et al., 1999; Bill et al., 2001; Parada et al., 2001; Hunter et al., 2004; Bortolotti and Principi, 2005; Lewandowski et al., 2005; Cordey and Bailly, 2007; Danelian et al.,

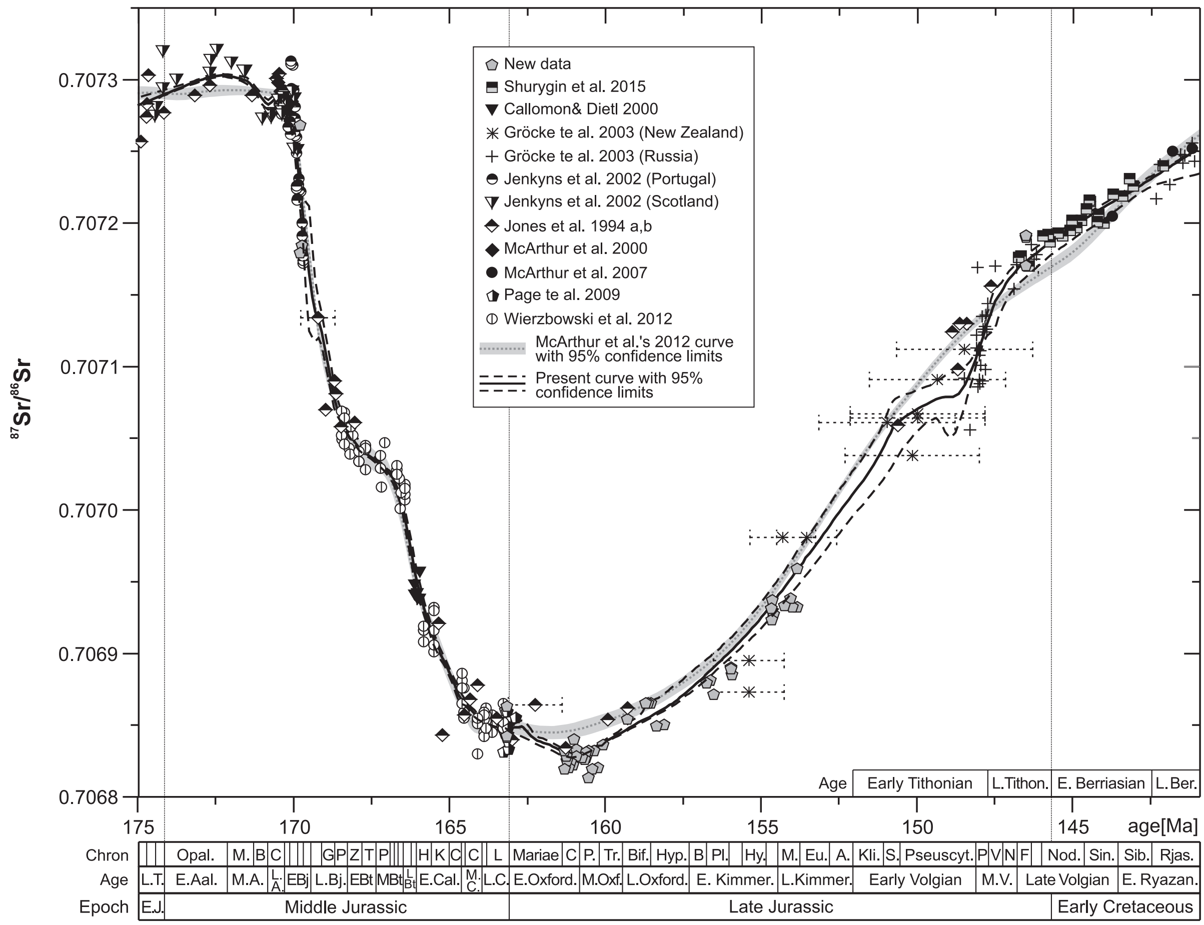

Fig. 9. Strontium isotope variations in the latest Early Jurassic–earliest Cretaceous. The Lowess curve (solid line), with given 95% confidence limits (dashed lines) is fitted to strontium isotope dataset of well-preserved fossils. The numerical time scale of the diagram is based on the data of Ogg et al. (2012, 2016). Dating errors higher than one subchron are marked. Dark grey dotted curve with light grey 95% confidence envelope – Sr isotope curve, version 5 of McArthur et al. (2012).

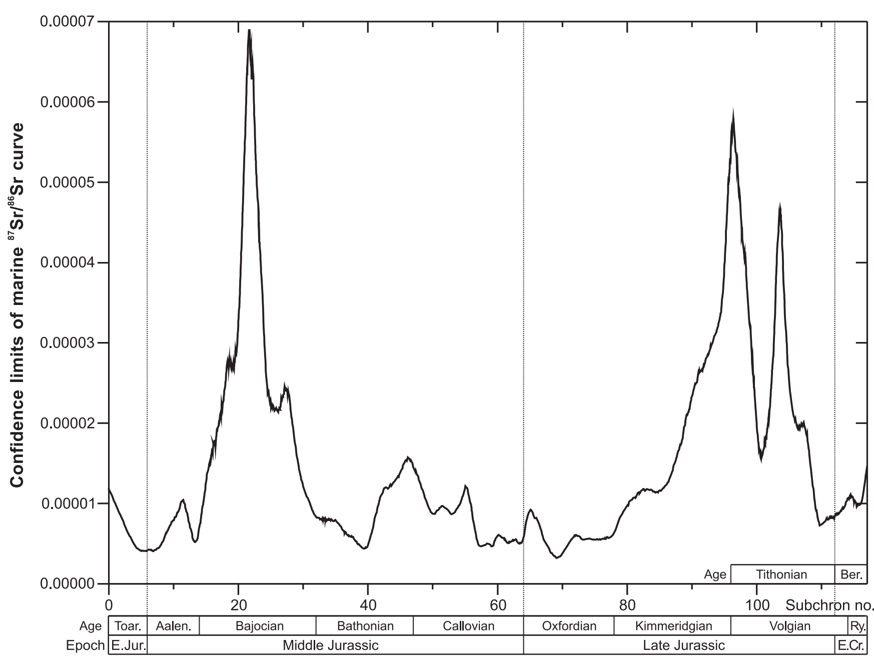

Fig. 10. Full-width of the 95% confidence limits (2 ∗ 2σ) of the fitted Middle–Late Jurassic seawater $^{87}Sr/^{86}Sr$ curve based on the biostratigraphical scale.

2008; Galoyan et al., 2009; Meijers et al., 2010; Bertok et al., 2011; Rubio-Cisneros and Lawton, 2011). The acceleration of spreading rates during the Middle Jurassic is confirmed by available geophysical data from the oceanic crust (Sheridan, 1997; Labails et al., 2010).

The pulse of volcanic activity of the ocean crust culminated in a well-documented global sea-level rise at the Middle–Late Jurassic transition, which is linked to the tectonic uplift of oceanic ridges, and the reorganization of the seafloor (Norris and Hallam, 1995; Jacquin

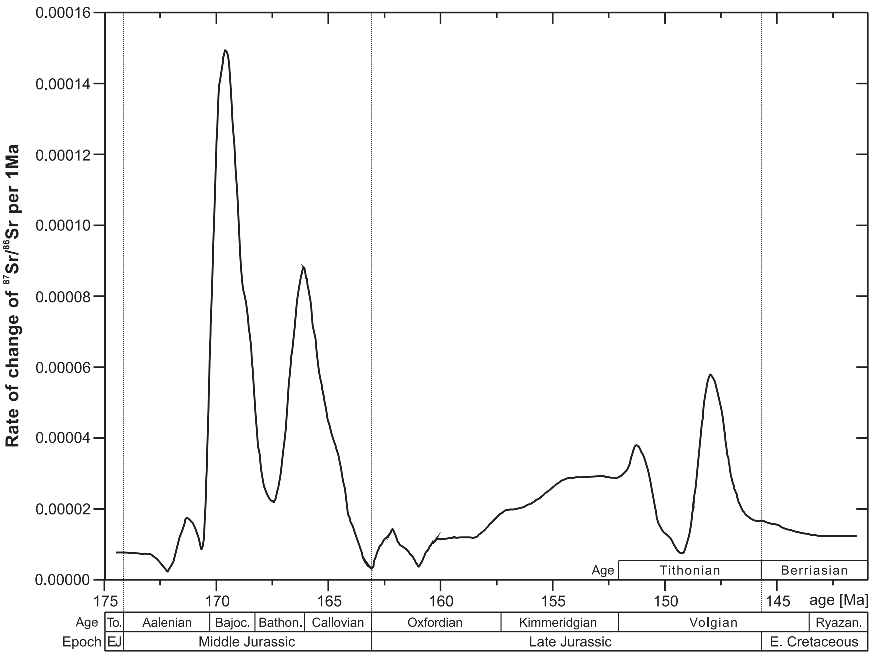

Fig. 11. Absolute rate of a change of seawater $^{87}Sr/^{86}Sr$ ratio per 1 Ma during the Middle–Late Jurassic. Running values calculated for seawater $^{87}Sr/^{86}Sr$ curve based on the numerical time scale.

et al., 1998; Hallam, 2001; Wierzbowski et al., 2009). The tectonically induced global sea-level rise, along with opening of new seaways, contributed, in turn, to the worldwide demise of carbonate platforms (Dromart et al., 2003; Donnadieu et al., 2011), common occurrences of gaps in the sedimentary records (Rais et al., 2007; Wierzbowski et al., 2009), and unification of marine faunas over vast areas during the Middle–Late Jurassic transition (Matyja and Wierzbowski, 1995; Marchand and Thierry, 1997; Wierzbowski et al., 2013). Another unexpected result of the activity of the oceanic crust during the Middle Jurassic, and the Middle–Late Jurassic transition may be a recently recognized monster shift (30°) of a palaeopole occurring between 160 and 145 Ma (Kent and Irving, 2010; Kent et al., 2015). The shift was likely triggered by major mass redistribution on the Earth geoid (Kent et al., 2015), and might have been connected with the reconfiguration of spreading, and subduction zones owing to the breakup of Gondwana, and the formation of new oceanic basins.

A Late Jurassic increase in the seawater $^{87}Sr/^{86}Sr$ ratio from 0.70683 at the Early–Middle Oxfordian transition (160.8 Ma ago) to 0.70720 at the Jurassic–Cretaceous transition (145.7 Ma ago) is characterized by a moderate rate of change of up to 0.00006 per 1 Ma (Fig. 11). The rate of change was likely the highest during the Late Kimmeridgian–Middle Volgian (= Late Kimmeridgian–earliest Late Tithonian; 154.5 to 146.8 Ma ago), but non-linearity of this segment of the strontium isotope curve may point to some problems with numerical time scale or its biostratigraphical calibration (Fig. 9). It is worth noting that the rise of marine $^{87}Sr/^{86}Sr$ ratio continued till the earliest Late Barremian (129.0 Ma ago), where a maximal ratio of 0.70749 was reached (McArthur et al., 2012). The increase may result from the deceleration of the spreading rate and the hydrothermal activity of the oceanic crust after the initial breakup of Gondwana, and the formation of new oceanic basins. In fact, available geophysical data point to a gradual decrease of spreading rates in the Pacific Ocean during the Late Jurassic (Nakanishi et al., 1992; Ogg, 2012). The decrease in the spreading rate is also observed in the Central Atlantic starting from the Tithonian (Labails et al., 2010). Nevertheless, the Late Jurassic–Early Cretaceous rise in the seawater $^{87}Sr/^{86}Sr$ ratio is also postulated to be a result of enhanced continental weathering, due to an early uplift and erosion of the North America Western Cordillera (cf. Gröcke et al., 2003). Recent modelling of Kristall et al. (2017) also shows that the rise may be interpreted as resulting from increasing input of radiogenic, continental strontium.

Departures from linearity of apparently straight parts of the numerically calibrated Middle–Late Jurassic strontium isotope curve, e.g. in the Early–Middle Bathonian, and in the latest Early–Middle Volgian (= latest Early–earliest Late Tithonian) may result from wrong estimates of the duration of some chrons or subages assigned by the GTS2012 scale (cf. Fig. 9; see also discussion in McArthur et al., 2016). This may point to the necessity of verification of some numerical data, however, the effect of potential dating problems on a general shape of the Middle–Late Jurassic seawater strontium isotope curve seems be minor and negligible for analysis of its causal factors.

8. Conclusions

The present estimation of the marine $^{87}Sr/^{86}Sr$ curve, using a statistical LOWESS method, is established on both the biostratigraphical, and numerical age time scales. Due to the high reliability of the curve, and presented stratigraphical charts with interregional correlations, the data may be used for precise dating of marine sediments in various biogeoprovinces. Precision below an ammonite zone level (or < 0.2 Ma) is obtained for steeper parts of the Middle–Late Jurassic strontium isotope curve.

The Middle–Late Jurassic marine strontium isotope curve is trough-shaped (Figs. 8, 9). The seawater $^{87}Sr/^{86}Sr$ ratio remained close to 0.70730 at the Toarcian–Aalenian transition and started to fall in the Middle Aalenian. The rate of the fall was the largest in the Phanerozoic history of the Earth during the Bajocian (up to a 0.00015 $^{87}Sr/^{86}Sr$ ratio change per 1 Ma). The Phanerozoic minimum of the seawater $^{87}Sr/^{86}Sr$ ratio with the value of ca. 0.70683 is noted at the Early–Middle Oxfordian transition. This period was followed by a gradual increase of the ratio (up to ca. 0.70720 at the Jurassic–Cretaceous transition).

The Middle–Late Jurassic trough of the seawater strontium isotope curve is linked to the enhanced hydrothermal venting of the oceanic crust during initial, and relatively fast breakup of the Gondwana, and the formation of new Atlantic–Tethyan oceanic basins. The onset and acceleration of all the tectonic processes is deduced from ophiolites, rhyolitic magmas, stratigraphic data, and palaeomagnetic studies. Minimal values of seawater $^{87}Sr/^{86}Sr$ ratio at the Middle–Late Jurassic transition coincide with a global sea-level rise, and prominent palaeooceanographical and palaeoenvironmental changes.

Supplementary data to this article can be found online at http://dx.doi.org/10.1016/j.chemgeo.2017.06.015.

Acknowledgements

This study was supported by the grant no. 2014/13/B/ST10/02511 of the National Science Centre, Poland. Field work in Russia was supported by the grant no. 17-17-01171 of the Russian Science Foundation. We are indebted to H.C. Jenkyns for kindly supplying digital strontium isotope data measured from Portugal and Scotland samples (the data points are depicted on the diagram in Jenkyns et al., 2002). Two anonymous reviewers are thanked for positive reviews and suggested improvements.

References

Alberti, M., Fürsich, F.T., Pandey, D.K., 2012. The Oxfordian stable isotope record (δ^{18}O, δ^{13}C) of belemnites, brachiopods, and oysters from the Kachchh Basin (western India) and its potential for palaeoecologic, palaeoclimatic, and palaeogeographic reconstructions. Palaeogeogr. Palaeoclimatol. Palaeoecol. 344-345, 49–68. http://dx.doi.org/10.1016/j.palaeo.2012.05.018.

Arabas, A., 2016. Middle–Upper Jurassic stable isotope records and seawater temperature variations: new palaeoclimate data from marine carbonate and belemnite rostra (Pieniny Klippen Belt, Carpathians). Palaeogeogr. Palaeoclimatol. Palaeoecol. 446, 284–294. http://dx.doi.org/10.1016/j.palaeo.2016.01.033.

Banner, J.L., 1995. Application of the trace element and isotope geochemistry of strontium to studies of carbonate diagenesis. Sedimentology 42, 805–824. http://dx.doi.org/10.1111/j.1365-3091.1995.tb00410.x.

Banner, J.L., Hanson, G.N., 1990. Calculation of simultaneous isotopic and trace element variations during water-rock interactions with applications to carbonate diagenesis. Geochim. Cosmochim. Acta 54, 3123–3137. http://dx.doi.org/10.1016/0016-7037(90)90128-8.

Baraboshkin, E.J., 1999. Berriasian-Valanginian (Early Cretaceous) seeways of the Russian Platform basin and the problem of Boreal/Tethyan correlation. Geol. Carpath. 50, 5–20.

Baraboshkin, E.Yu, Rogov, M.A., Guzhikov, A.Yu, Dzyuba, O.S., Urman, O.S., Shurygin, B.N., Pestchevitskaya, E.B., Manikin, A.G., 2016. Kashpir section (Volga River, Russia), the proposed auxiliary section for the J/K interval in Subboreal Realm. In: XIIth Jurassica Conference. Workshop of the ICS Berriasian Group and IGCP 632. Field Trip Guide and Abstracts Book, Smolenice, Slovakia, April 19–23, 2016. Earth Science Institute, Slovak Academy of Sciences, Bratislava, pp. 109–112.

Basu, A.R., Jacobsen, S.B., Poreda, R.J., Dowling, C.B., Aggarwal, P.K., 2001. Large groundwater strontium flux to the oceans from the Bengal Basin and the marine strontium isotope record. Science 293, 1470–1473. http://dx.doi.org/10.1126/science.1060524.

Bertok, C., Martire, L., Perotti, E., d'Atri, A., Piana, F., 2011. Middle–Late Jurassic syndepositional tectonics recorded in the Ligurian Briançonnais succession (Marguareis–Mongioie area, Ligurian Alps, NW Italy). Swiss J. Geosci. 104, 237–255. http://dx.doi.org/10.1007/s00015-011-0058-0.

Bill, M., O'Dogherty, L., Guex, J., Baumgartner, P.O., Masson, H., 2001. Radiolarite ages in Alpine-Mediterranean ophiolites: constraints on the oceanic spreading and the Tethys-Atlantic connection. GSA Bull. 113, 129–143. http://dx.doi.org/10.1130/0016-7606(2001)113 < 0129:RAIAMO > 2.0.CO;2.

Bortolotti, V., Principi, G., 2005. Tethyan ophiolites and Pangea break-up. Island Arc 14, 442–470. http://dx.doi.org/10.1111/j.1440-1738.2005.00478.x.

Bragin, N. Yu, Kiselev, D.N., 2013. Radiolarians from Upper Jurassic (Middle Oxfordian and Upper Kimmeridgian) deposits of Yaroslavl Oblast. Stratigr. Geol. Correl. 21, 628–636.

Bragin, V.Yu., Dzyuba, O.S., Kazansky, A.Yu., Shurygin, B.N., 2013. New data on the magnetostratigraphy of the Jurassic–Cretaceous boundary interval, Nordvik Peninsula (northern East Siberia). Russ. Geol. Geophys. 54, 335–348. http://dx.doi.org/10.1016/j.rgg.2013.02.008.

Brand, U., Veizer, J., 1980. Chemical diagenesis of a multicomponent carbonate system-1: Trace elements. J. Sediment. Petrol. 50, 1219–1236. http://dx.doi.org/10.1306/212F7BB7-2B24-11D7-8648000102C1865D.

Brassier, M., Geleta, S., 1993. A planktonic marker and Callovian–Oxfordian fragmentation of Gondwana: data from Ogaden Basin, Ethiopia. Palaeogeogr. Palaeoclimatol. Palaeoecol. 104, 177–184. http://dx.doi.org/10.1016/0031-0182(93)90129-7.

Bryant, J.D., Jones, D.S., Mueller, P.A., 1995. Influence of freshwater flux on ^{87}Sr/^{86}Sr chronostratigraphy in marginal marine environments and dating of vertebrate and invertebrate faunas. J. Paleontol. 69, 1–6. http://dx.doi.org/10.1017/S002233600002686X.

Callomon, J.H., Dietl, G., 2000. On the proposed basal boundary stratotype (GSSP) of the Middle Jurassic Callovian Stage. Geores. Forum 6, 41–54.

Cleveland, W.S., 1979. Robust locally weighted regression and smoothing scatterplots. J. Am. Stat. Assoc. 74, 829–836.

Cordey, F., Bailly, A., 2007. Alpine ocean seafloor spreading and onset of pelagic sedimentation: new radiolarian data from the Chenaillet-Montgenèvre ophiolite (French-Italian Alps). Geodin. Acta 20, 131–138. http://dx.doi.org/10.3166/ga.20.131-138.

Danelian, T., De Wever, P., Durand-Delga, M., 2008. Revised radiolarian ages for the sedimentary cover of the Balagne ophiolite (Corsica, France). Implications for the palaeoenvironmental evolution of the Balano-Ligurian margin. Bull. Soc. Geol. Fr. 179, 289–296. http://dx.doi.org/10.2113/gssgfbull.179.3.289.

Davis, A.C., Bickle, M.J., Teagle, D.A.H., 2003. Imbalance in the oceanic strontium budget. Earth Planet. Sci. Lett. 211, 173–187. http://dx.doi.org/10.1016/S0012-821X(03)00191-2.

Donnadieu, Y., Dromart, G., Goddéris, Y., Pucéat, E., Brigaud, B., Dera, G., Dumas, C., Oliver, N., 2011. A mechanism for brief glacial episodes in the Mesozoic greenhouse. Paleoceanography 26, PA3212. http://dx.doi.org/10.1029/2010PA002100.

Dromart, G., Garcia, J.-P., Gaumet, F., Picard, S., Rousseau, M., Atrops, F., Lecuyer, C., Sheppard, S.M.F., 2003. Perturbation of the carbon cycle at the Middle/Late Jurassic transition: geological and geochemical evidence. Am. J. Sci. 303, 667–707. http://dx.doi.org/10.2475/ajs.303.8.667.

Dzyuba, O.S., Izokh, O.P., Shurygin, B.N., 2013. Carbon isotope excursions in Boreal Jurassic–Cretaceous boundary sections and their correlation potential. Palaeogeogr. Palaeoclimatol. Palaeoecol. 381-382, 33–46. http://dx.doi.org/10.1016/j.palaeo.2013.04.013.

Elderfield, H., 1986. Strontium isotope stratigraphy. Palaeogeogr. Palaeoclimatol. Palaeoecol. 57, 71–90. http://dx.doi.org/10.1016/0031-0182(86)90007-6.

Faure, G., 1986. Principles of Isotope Geology, second edition. John Wiley & Sons, New York/Chichester/Brisbane/Toronto/Singapore (589 pp).

Féraud, G., Alric, V., Fornari, M., Bertrand, H., Haller, M., 1999. ^{40}Ar/^{39}Ar dating of the Jurassic volcanic province of Patagonia: migrating magmatism related to Gondwana break-up and subduction. Earth Planet. Sci. Lett. 172, 83–96. http://dx.doi.org/10.1016/S0012-821X(99)00190-9.

Gallois, R.W., 2011. A revised description of the lithostratigraphy of the Kimmeridgian-Tithonian and Kimmeridgian-Volgian boundary beds at Kimmeridge, Dorset, UK. Geosci. South-West Engl. 12, 288–294.

Gallois, R.W., 2012. A revised description of the lithostratigraphy of the Kimmeridgian-Tithonian and Kimmeridgian-Volgian boundary beds at Kimmeridge, Dorset, UK: reply to Wimbledon 2012. Geosci. South-West Engl. 13, 132–134.

Galoyan, G., Rolland, Y., Sosson, M., Corsini, M., Billo, S., Verati, C., Melkonyan, R., 2009. Geology, geochemistry and ^{40}Ar/^{39}Ar dating of Sevan ophiolites (Lesser Caucasus, Armenia): evidence for Jurassic Back-arc opening and hot spot event between South Armenian Block and Eurasia. J. Asian Earth Sci. 135–153. http://dx.doi.org/10.1016/j.jseaes.2008.04.002.

Głowniak, E., 1997. The Philogenesis, Taxonomy and Stratigraphic Meaning of the Middle Oxfordian Perisphinctid Ammonites From the Polish Jura Chain. Institute of Geology, University of Warsaw, Warsaw (PhD thesis, in Polish).

Głowniak, E., 2000. The *Platysphinctes* immigration event in the Middle Oxfordian of the Polish Jura Chain (Central Poland). Acta Geol. Pol. 50, 143–160.

Głowniak, E., 2002. The ammonites of the family Perisphinctidae from the Plicatilis Zone (lower Middle Oxfordian) of the Polish Jura Chain (Central Poland); their taxonomy, phylogeny and biostratigraphy. Acta Geol. Pol. 52, 307–364.

Głowniak, E., 2006. Correlation of the zonal schemes at the Middle–Upper Oxfordian (Jurassic) boundary in the Submediterranean Province: Poland and Switzerland. Acta Geol. Pol. 56, 33–50.

Głowniak, E., Kiselev, D.N., Rogov, M., Wierzbowski, A., Wright, J.K., 2010. The Middle Oxfordian to lowermost Kimmeridgian ammonite succession at Mikhalenino (Kostroma District) of the Russian Platform, and its stratigraphical and palaeobiogeographical importance. Vol. Jur. 8, 5–48.

Gradstein, F.M., 2012. Introduction. In: Gradstein, F.M., Ogg, J.G., Schmitz, M., Ogg, G. (Eds.), The Geologic Time Scale 2012. Elsevier, Amsterdam, Boston, Heidelberg, London, New York, Oxford, Paris, San Diego, San Francisco, Singapore, Sydney, Tokyo, pp. 1–29.

Gradstein, F.M., Gibling, M.R., Sarti, M., Von Rad, U., Thurow, J.W., Ogg, J.G., Jansa, L.F., Kaminski, M.A., Westermann, G.E.G., 1991. Mesozoic Tethyan strata of Thakkhola, Nepal: evidence for the drift and breakup of Gondwana. Palaeogeogr. Palaeoclimatol. Palaeoecol. 88, 193–218. http://dx.doi.org/10.1016/0031-0182(91)90065-Y.

Gradstein, F.M., Ogg, J.G., Smith, A.G., et al., 2004. A Geologic Time Scale 2004. Cambridge University Press, Cambridge, New York, Melbourne, Madrid, Cape Town, Singapore, São Paulo (589 pp).

Gröcke, D.R., Price, G.D., Ruffell, A.H., Mutterlose, J., Baraboshkin, E., 2003. Isotopic evidence for Late Jurassic–Early Cretaceous climate change. Palaeogeogr. Palaeoclimatol. Palaeoecol. 202, 97–118. http://dx.doi.org/10.1016/S0031-0182(03)00631-X.

Groupe Français d'Étude du Jurassique (coordinated by Cariou, E., and Hantzpergue, P.), 1997. Biostratigraphie du Jurassique ouest-européen et méditerranéen: zonations parallèles et distribution des invertébrés et microfossiles. In: Bulletin des Centres de Recherches Exploration- Production Elf-Aquitaine, Mémoire 17, pp. 422.

Hallam, A., 2001. A review of the broad pattern of Jurassic sea-level changes and their possible causes in the light of current knowledge. Palaeogeogr. Palaeoclimatol. Palaeoecol. 167, 23–37. http://dx.doi.org/10.1016/S0031-0182(00)00229-7.

Hercman, H., 2009. Age ~ depth model construction using full information from samples age and depth distributions basing on ^{230}Th/U radiocarbon and ^{210}Pb dating results. In: 15th International Congress of Speleology. Kerville, Texas, 19-26.07.2009, pp. 1024–1025.

Hercman, H., Pawlak, J., 2012. MOD-AGE: an age-depth model construction algorithm. Quat. Geochronol. 12, 1–10. http://dx.doi.org/10.1016/j.quageo.2012.05.003.

Houša, V., Pruner, P., Zakharov, V.A., Kostak, M., Chadima, M., Rogov, M.A., Šlechta, S., Mazuch, M., 2007. Boreal–Tethyan correlation of the Jurassic–Cretaceous boundary interval by magneto- and biostratigraphy. Stratigr. Geol. Correl. 15, 297–309. http://dx.doi.org/10.1134/S0869593807030057.

Howarth, R.J., McArthur, J.M., 1997. Statistics for strontium isotope stratigraphy: a robust LOWESS fit to the marine Sr-isotope curve for 0 to 206 Ma, with look-up table for derivation of numerical age. J. Geol. 105, 441–456. http://dx.doi.org/10.1086/515938.

Hunter, M.A., Riley, T.R., Millar, I.L., 2004. Middle Jurassic air fall tuff in the sedimentary Latady Formation, eastern Ellsworth Land. Antarct. Sci. 16, 185–190. http://dx.doi.org/10.1017/S0954102004001944.

Imai, N., Terashima, S., Itoh, S., Ando, A., 1996. 1996 compilation of analytical data on nine GSJ geochemical reference samples, "sedimentary rock series". Geostand. Geoanal. Res. 20, 165–216.

Jacquin, T., Dardeau, G., Durlet, C., Graciansky, P.-C., Hantzpergue, P., 1998. The North Sea cycle: an overview of 2nd order transgressive/regressive facies cycles. In: de Graciansky, P.-C., Hardenbol, J., Jacquin, T., Vail, P.R. (Eds.), Western Europe, In: Mesozoic and Cenozoic Sequence Stratigraphy of European Basins. No. 60. SEPM (Society for Sedimentary Geology) Special Publication, pp. 445–466.

Jenkyns, H.C., Jones, C.E., Gröcke, D.R., Hesselbo, S.P., Parkinson, D.N., 2002. Chemostratigraphy of the Jurassic System: applications, limitations and implications for palaeoceanography. J. Geol. Soc. Lond. 159, 351–378. http://dx.doi.org/10.1144/0016-764901-130.

Jones, C.E., Jenkyns, H.C., 2001. Seawater strontium isotopes, oceanic anoxic events, and seafloor hydrothermal activity in the Jurassic and Cretaceous. Am. J. Sci. 301, 112–149. http://dx.doi.org/10.2475/ajs.301.2.112.

Jones, C.E., Jenkyns, H.C., Coe, A.L., Hesselbo, S.P., 1994a. Strontium isotopic variations in Jurassic and Cretaceous seawater. Geochim. Cosmochim. Acta 58, 3061–3074. http://dx.doi.org/10.1016/0016-7037(94)90179-1.

Jones, C.E., Jenkyns, H.C., Hesselbo, S.P., 1994b. Strontium isotopes in Early Jurassic seawater. Geochim. Cosmochim. Acta 58, 1285–1301. http://dx.doi.org/10.1016/0016-7037(94)90382-4.

Kent, D.V., Irving, E., 2010. Influence of inclination error in sedimentary rocks on the Triassic and Jurassic apparent pole wander path of North America and implications for Cordilleran tectonics. J. Geophys. Res. 115, B10103. http://dx.doi.org/10.1029/2009JB007205.

Kent, D.V., Kjarsgaard, B.A., Gee, J.S., Muttoni, G., Heaman, L.M., 2015. Tracking the Late Jurassic apparent (or true) polar shift in U-Pb-dated kimberlites from cratonic North America (Superior Province of Canada). Geochem. Geophys. Geosyst. 16, 983–994. http://dx.doi.org/10.1002/2015GC005734.

Kiselev, D.N., 2003. Ioda. In: Fedorov, V.M., Labutin, D.I., Timoshenko, N.F., Maslov, I.A., Poyarkov, B.V., Novikov, I.V., Vorontsov, A.K., Kiselev, D.N., Baranov, V.N., Muravin, E.S., Sennikov, A.G. (Eds.), Atlas of the Yaroslavl Region Geological Monuments. Pedagogical University of Yaroslavl. Palaeontological Institute, Russian Academy of Sciences. Administration of Yaroslavl Region, Natural Resources Ministry of Russia, pp. 45–50 (In Russian).

C. Korte, C.V. Ullmann. Permian strontium isotope stratigraphy. The Permian Timescale, Geological Society Special Publications. 450 http://dx.doi.org/10.1029/2009GC002869 (in press).

Krabbenhöft, A., Eisenhauer, A., Böhm, F., Vollstaedt, H., Fietzke, J., Liebetrau, V., Augustin, N., Peucker-Ehrenbrink, B., Müller, M.N., Horn, C., Hansen, B.T., Nolte, N., Wallmann, K., 2010. Constraining the marine strontium budget with natural strontium isotope fractionations ($^{87}Sr/^{86}Sr^*$, $\delta^{88/86}Sr$) of carbonates, hydrothermal solutions and river waters. Geochim. Cosmochim. Acta 74, 4097–4109. http://dx.doi.org/10.1016/j.gca.2010.04.009.

Kristall, B., Jacobson, A.D., Hurtgen, M.T., 2017. Modeling the paleo-seawater radiogenic strontium isotope record: a case study of the Late Jurassic–Early Cretaceous. Palaeogeogr. Palaeoclimatol. Palaeoecol. 472, 163–176. http://dx.doi.org/10.1016/j.palaeo.2017.01.048.

Kutek, J., Zeiss, A., 1997. The highest Kimmeridgian and Lower Volgian in Central Poland; their ammonites and biostratigraphy. Acta Geol. Pol. 47, 107–198.

Kuznetsov, A.B., Semikhatov, M.A., Gorokhov, I.M., 2012. The Sr isotope composition of the World Ocean, marginal and inland seas: implications for the Sr isotope stratigraphy. Stratigr. Geol. Correl. 20, 501–515. http://dx.doi.org/10.1134/S0869593812060044.

Labails, C., Olivet, J.-L., Aslanian, D., Roest, W.R., 2010. An alternative early opening scenario for the Central Atlantic Ocean. Earth Planet. Sci. Lett. 297, 355–368. http://dx.doi.org/10.1016/j.epsl.2010.06.024.

Lakova, I., Petrova, S., 2013. Towards a standard Tithonian to Valanginian calpionellid zonation of the Tethyan Realm. Acta Geol. Pol. 63, 201–221. http://dx.doi.org/10.2478/agp-2013-0008.

Lewandowski, M., Krobicki, M., Matyja, B.A., Wierzbowski, A., 2005. Palaeogeographic evolution of the Pieniny Klippen Basin using stratigraphic and palaeomagnetic data from the Veliky Kamenets section (Carpathians, Ukraine). Palaeogeogr. Palaeoclimatol. Palaeoecol. 216, 53–72. http://dx.doi.org/10.1016/j.palaeo.2004.10.002.

Marchand, D., Thierry, J., 1997. Enregistrement des variations morphologiques et de la composition des peuplements d'ammonites durant le cycle régressif/transgressif de 2ème ordre Bathonian inférieur–Oxfordian inférieur en Europe Occidentale. Bull. Soc. Geol. Fr. 168, 121–132.

Marshall, J.D., 1992. Climatic and oceanographic isotopic signals from the carbonate rock record and their preservation. Geol. Mag. 129, 143–160. http://dx.doi.org/10.1017/S0016756800008244.

Matyja, B.A., Wierzbowski, A., 1995. Biogeographic differentiation of the Oxfordian and Early Kimmeridgian ammonite faunas of Europe, and its stratigraphic consequences. Acta Geol. Pol. 45, 1–8.

Matyja, B.A., Wierzbowski, A., 2000a. Ammonites and stratigraphy of the uppermost Bajocian and Lower Bathonian between Częstochowa and Wieluń, Central Poland. Acta Geol. Pol. 50, 191–209.

Matyja, B.A., Wierzbowski, A., 2000b. Biostratigraphical correlations between the Subboreal Muatbilis Zone and the Submediterranean Upper Hypselocyclum – Divisum zones of the Kimmeridgian: new data from Northern Poland. Geores. Forum 6, 129–136.

Matyja, B.A., Wierzbowski, A., 2016. Ammonites and ammonite stratigraphy of the uppermost Jurassic (Tithonian) of the Owadów–Brzezinki quarry (central Poland). Volumina Jurassica 14, 65–122. http://dx.doi.org/10.5604/17313708.1219562.

McArthur, J.M., 1994. Recent trends in strontium isotope stratigraphy. Terra Nova 6, 331–358. http://dx.doi.org/10.1111/j.1365-3121.1994.tb00507.x.

McArthur, J.M., Morton, N., Thirlwall, M.F., 2000. Strontium isotope startigraphy of the Aalenian/Bajocian auxiliary stratotype point at Bearreraig, Isle of Skye, NW Scotland. Geores. Forum 6, 137–144.

McArthur, J.M., Howarth, R.J., Bailey, T.R., 2001. Strontium isotope stratigraphy: LOWESS version 3: best fit to the marine Sr-isotope curve for 0–509 Ma and accompanying look-up table for deriving numerical age. J. Geol. 109, 155–170. http://dx.doi.org/10.1086/319243.

McArthur, J.M., Janssen, N.M.M., Reboulet, S., Leng, M.J., Thirlwall, M.F., van de Schootbrugge, B., 2007. Palaeotemperatures, polar ice-volume, and isotope stratigraphy (Mg/Ca, $\delta^{18}O$, $\delta^{13}C$, $^{87}Sr/^{86}Sr$): the Early Cretaceous (Berriasian, Valanginian, Hauterivian). Palaeogeogr. Palaeoclimatol. Palaeoecol. 248, 391–430. http://dx.doi.org/10.1016/j.paleo.2006.12.015.

McArthur, J.M., Howarth, R.J., Shields, G.A., 2012. Strontium isotope stratigraphy. In: Gradstein, F.M., Ogg, J.G., Schmitz, M., Ogg, G. (Eds.), The Geologic Time Scale 2012. Elsevier, Amsterdam, Boston, Heidelberg, London, New York, Oxford, Paris, San Diego, San Francisco, Singapore, Sydney, Tokyo, pp. 127–144.

McArthur, J.M., Steuber, T., Page, K.N., Landmann, N.H., 2016. Sr-isotope stratigraphy: assigning time in the Campanian, Pliensbachian, Toarcian, and Valanginian. J. Geol. 124, 569–586. http://dx.doi.org/10.1086/687395.

Meijers, M.J.M., Vrouwe, B., van Hinsbergen, D.J.J., Kuiper, K.F., Wijbrans, J., Davies, G.R., Stephenson, R.A., Kaymakci, N., Matenco, L., Saintot, A., 2010. Jurassic arc volcanism on Crimea (Ukraine): implications for the paleo-subduction zone configuration of the Black Sea region. Lithos 119, 412–426. http://dx.doi.org/10.1016/j.lithos.2010.07.017.

Mitta, V.V., 2005. New data on the age of the Ryazanian stage basal layers. Stratigr. Geol. Correl. 13, 503–511.

Mitta, V.V., 2007. Ammonite assemblages from basal layers of the Ryazanian Stage (Lower Cretaceous) of Central Russia. Stratigr. Geol. Correl. 15, 193–205. http://dx.doi.org/10.1134/S0869593807020050.

Nakanishi, M., Tamaki, K., Kobayashi, K., 1992. Magnetic anomaly lineations from Late Jurassic to Early Cretaceous in the west-central Pacific Ocean. Geophys. J. Int. 109, 701–719. http://dx.doi.org/10.1111/j.1365-246X.1992.tb00126.x.

Nier, A.O., 1938. The isotopic constitution of strontium, barium, bismuth, thallium and mercury. Phys. Rev. 54, 275–278. http://dx.doi.org/10.1103/PhysRev.54.275.

Norris, M.S., Hallam, A., 1995. Facies variations across the Middle–Upper Jurassic boundary in Western Europe and the relationship to sea-level changes. Palaeogeogr. Palaeoclimatol. Palaeoecol. 116, 189–245. http://dx.doi.org/10.1016/0031-0182(94)00096-Q.

Nunn, E.V., Price, G.D., Hart, M.B., Page, K.N., Leng, M.J., 2009. Isotopic signals from Callovian–Kimmeridgian (Middle–Upper Jurassic) belemnites and bulk organic carbon, Staffin Bay, Isle of Skye, Scotland. J. Geol. Soc. Lond. 166, 633–641. http://dx.doi.org/10.1144/0016-76492008-067.

Ogg, J.G., 2012. Geomagnetic polarity time scale. In: Gradstein, F.M., Ogg, J.G., Schmitz, M., Ogg, G. (Eds.), The Geologic Time Scale 2012. Elsevier, Amsterdam, Boston, Heidelberg, London, New York, Oxford, Paris, San Diego, San Francisco, Singapore, Sydney, Tokyo, pp. 85–113.

Ogg, J.G., Hinnov, L.A., Huang, C., 2012. Jurassic. In: Gradstein, F.M., Ogg, J.G., Schmitz, M., Ogg, G. (Eds.), The Geologic Time Scale 2012. Elsevier, Amsterdam, Boston, Heidelberg, London, New York, Oxford, Paris, San Diego, San Francisco, Singapore, Sydney, Tokyo, pp. 731–791.

Ogg, J.G., Ogg, G.M., Gradstein, F.M., 2016. A Concise Geologic Time Scale. Elsevier, Amsterdam, Boston, Heidelberg, London, New York, Oxford, Paris, San Diego, San Francisco, Singapore, Sydney, Tokyo (234 pp).

Page, K.N., Meléndez, G., Hart, M.B., Price, G.D., Wright, J.K., Bown, P., Bello, J., 2009. Integrated stratigraphical study of the candidate Oxfordian Global Stratotype Section and Point (GSSP) at Redcliff Point, Weymouth, Dorset, UK. Vol. Jur. 7, 101–111.

Parada, M.A., Lahsen, A., Palacios, C., 2001. Ages and geochemistry of Mesozoic-Eocene back-arc volcanic rocks in the Aysén region of the Patagonian Andes, Chile. Rev. Geol. Chile 28, 25–46. http://dx.doi.org/10.4067/S0716-02082001000100002.

Pearce, C.R., Parkinson, I.J., Gaillardet, J., Charlier, B.L.A., Mokadem, F., Burton, K.W., 2015. Reassesing the stable ($\delta^{88/86}Sr$) and radiogenic ($^{87}Sr/^{86}Sr$) strontium isotopic composition of marine inputs. Geochim. Cosmochim. Acta 157, 125–146. http://dx.doi.org/10.1016/j.gca.2015.02.029.

Peucker-Ehrenbrink, B., Miller, M.W., Arsouze, T., Jeandel, C., 2010. Continental bedrock and riverine fluxes of strontium and neodymium isotopes to the oceans. Geochem. Geophys. Geosyst. 11, Q03016. http://dx.doi.org/10.1029/2009GC002869.

Podlaha, O.G., Mutterlose, J., Veizer, J., 1998. Preservation of $\delta^{18}O$ and $\delta^{13}C$ in belemnite rostra from the Jurassic/Early Cretaceous successions. Am. J. Sci. 298, 324–347. http://dx.doi.org/10.2475/ajs.298.4.324.

Pszczółkowski, A., 2016. The Tithonian Chitinoidellidae and other microfossils from Owadów–Brzezinki quarry (central Poland). Vol. Jur. 14, 133–144. http://dx.doi.org/10.5604/17313708.1222642.

Rais, P., Louis-Schmid, B., Bernasconi, S.M., Weissert, H., 2007. Palaeoceanographic and palaeoclimatic reorganization around the Middle–Late Jurassic transition. Palaeogeogr. Palaeoclimatol. Palaeoecol. 251, 527–546. http://dx.doi.org/10.1016/j.palaeo.2007.05.008.

Rioult, M., Contini, D., Elmi, S., Gabilly, J., Mouterde, R., 1997. Biostratigraphie du Jurassique Ouest-Européen et Méditerranéen: zonations parallèles et distribution des invertébrés et microfossiles. In: Cariou, E., Hantzpergue, P. (Eds.), 6 – Bajocien. Bulletin du Centre de Recherches Elf Exploration Production, Mémoire, 17pp. 41–53.

Rogov, M.A., 2004. The Russian Platform as a key region for Volgian/Tithonian correlation: a review of the Mediterranean faunal elements and ammonite biostratigraphy of the Volgian stage. Riv. Ital. Paleontol. Stratigr. 110, 321–328.

Rogov, M.A., 2010a. A precise ammonite biostratigraphy through the Kimmeridgian-Volgian boundary beds in the Gorodischi section (Middle Volga area, Russia), and the

base of the Volgian Stage in its type area. Vol. Jur. 8, 103–130.
Rogov, M.A., 2010b. New data on ammonites and stratigraphy of the Volgian Stage in Spitzbergen. Stratigr. Geol. Correl. 18, 505–531. http://dx.doi.org/10.1134/S0869593810050047.
Rogov, M.A., 2011. On the Kimmeridgian-Volgian boundary. In: Shurygin, B.N., Lebedeva, N.K., Goryacheva, A.A. (Eds.), Palaeontology, Stratigraphy and Palaeogeography of Mesozoic and Cenozoic of Boreal Basins. Materials of Scientific Session (18–22 April, 2011), In 2 Volumes. Vol. I. Mesozoic IPGG SB RAS, Novosibirsk, pp. 245–248 (in Russian).
Rogov, M.A., 2013. Ammonites and infrazonal subdivision of the *Dorsoplanites panderi* Zone (Volgian Stage, Upper Jurassic) of the European part of Russia. Dokl. Earth Sci. 451, 803–808. http://dx.doi.org/10.1134/S1028334X13080059.
Rogov, M., 2014. Infrazonal subdivision of the Volgian Stage in its type area using ammonites and correlation of the Volgian and Tithonian Stages. In: Rocha, R., Pais, J., Kullberg, J.C., Finney, S. (Eds.), STRATI 2013. First International Congress on Stratigraphy. At the Cutting Edge of Stratigraphy. Springer Geology, Springer International Publishing, Switzerland, pp. 577–580. http://dx.doi.org/10.1007/978-3-319-04364-7_111.
Rogov, M.A., Starodubtseva, I.A., 2014. The Khoroshevo Section (Moscow) - «Palaeontological Klondike» of XIX century, and its significance for studying of ammonites and stratigraphy of Volgian Stage. Byull. Mosk. Obshch. Ispyt. Prir. Otd. Geol. 89, 16–33.
Rogov, M., Zakharov, V., 2009. Ammonite- and bivalve-based biostratigraphy and Panboreal correlation of the Volgian Stage. Sci. China Ser. D Earth Sci. 52, 1890–1909. http://dx.doi.org/10.1007/s11430-009-0182-0.
Rogov, M.A., Wierzbowski, A., Shchepetova, E.V., Wierzbowski, H., 2014. New data on the Lower–Upper Kimmeridgian boundary beds of southern Tatarstan, Central Russia. In: Pandey, D.K., Fürsich, F.T., Alberti, M. (Eds.), 9th International Congress on the Jurassic System, Jaipur, India. Abstracts. Beringeria Special Issue 8, Erlangen, pp. 174–175.
Rogov, M.A., Baraboshkin, E.Yu., Guzhikov, A.Yu., Efimov, V.M., Kiselev, D.N., Morov, V.P., Gusev, V.V., 2015a. The Jurassic-Cretaceous boundary in the Middle Volga region. In: Field Guide to the International Meeting on the Jurassic/Cretaceous Boundary. September 7–13, 2015, Samara (Russia). Samara State Technical University, Samara (130 pp).
Rogov, M.A., Alifirov, A.S., Igolnikov, A.E., 2015b. Revised ammonite succession of the Upper Volgian of Nordvik section: zonal boundaries and uncertainties. In: The International Scientific Conference on the Jurassic/Cretaceous Boundary. Proceedings Volume. September 7–13, 2015, Samara (Russia). Kassandra, Togliatti, pp. 70–76.
Rogov, M.A., Ershova, V.B., Shchepetova, E.V., Zakharov, V.A., Pokrovsky, B.G., Khudoley, A.K., 2017. Earliest Cretaceous (late Berriasian) glendonites from Northeast Siberia revise the timing of initiation of transient Early Cretaceous cooling in the high latitudes. Cretac. Res. 71, 102–112. http://dx.doi.org/10.1016/j.cretres.2016.11.011.
Rogov, M.A., Wierzbowski, A., Shchepetova, E.V., 2017. Ammonite assemblages in the Lower to Upper Kimmeridgian boundary interval (Cymodoce to Mutabils zones) of Tatarstan (central European Russia) and their correlation importance. N. Jb. Geol. Paläont. A (in press).
Rubio-Cisneros, I.I., Lawton, T.F., 2011. Detrital zircon U-Pb ages of sandstones in continental red beds at Valle de Huizachal, Tamaulipas, NE Mexico: record of Early-Middle Jurassic arc volcanism and transition to crustal extension. Geosphere 7, 159–170. http://dx.doi.org/10.1130/GES00567.1.
Russell, W.A., Papanastassiou, D.A., Tombrello, T.A., 1978. Ca isotope fractionation on the Earth and other solar system materials. Geochim. Cosmochim. Acta 42, 1075–1090. http://dx.doi.org/10.1016/0016-7037(78)90105-9.
Sælen, G., 1989. Diagenesis and construction of the belemnite rostrum. Palaeontology 32, 765–798.
Sandoval, J., O'Dogherty, L., Vera, J.A., Guex, J., 2002. Sea-level changes and ammonite faunal turnover during the Lias/Dogger transition in the western Tethys. Bull. Soc. Geol. Fr. 173, 57–66. http://dx.doi.org/10.2113/173.1.57.
Savard, M.M., Veizer, J., Hinton, R., 1995. Cathodoluminescence at low Fe and Mn concentrations: a SIMS study of zones in natural calcites. J. Sediment. Res. A65, 208–213. http://dx.doi.org/10.1306/D4268072-2B26-11D7-8648000102C1865D.
Scherzinger, A., Schweigert, G., Főzy, I., 2016. First record of the Mediterranean zonal index *Mesosimoceras cavouri* (Gemmellaro, 1872) in the Upper Jurassic (Pseudomutabilis Zone, *semicostatum* γ horizon) of SW Germany and its stratigraphical significance. Vol. Jur. 14, 145–154. http://dx.doi.org/10.5604/01.3001.0009.4020.
Schnabl, P., Pruner, P., Wimbledon, W.A.P., 2015. A review of magnetostratigraphic results from the Tithonian–Berriasian of Nordvik (Siberia) and possible biostratigraphic constraints. Geol. Carpath. 66, 489–498. http://dx.doi.org/10.1515/geoca-2015-0040.
Schneider, S., Fürsich, F.T., Werner, W., 2009. Sr-isotope stratigraphy of the Upper Jurassic of central Portugal (Lusitanian Basin) based on oyster shells. Int. J. Earth Sci. 98, 1949–1970. http://dx.doi.org/10.1007/s00531-008-0359-3.
Schweigert, G., Callomon, J.H., 1997. Der bauhini-Faunenhorizont und seine Bedeutung für die Korrelation zwischen tethyalem und subborealem Oberjura. Stuttg. Beitr. Naturkunde B247, 1–69.
Segit, T., 2010. Stratigraphy, Facies Variability and Sedimentary Environment of the Aalenian and Lower Bajocian of the Pieniny Klippen Basin in Some Polish and Slovakian Sections. Faculty of Geology, University of Warsaw (unpublished Ph. D. Thesis, in Polish).
Shchepetova, E.V., Rogov, M.A., 2013. Organic carbon rich horizons in Upper Kimmeridgian of the northern part of Ulyanovsk-Saratov trough (Russian Platform): biostratigraphy, sedimentology and geochemistry. In: Zakharov, V.A., Rogov, M.A., Shurygin, B.N. (Eds.), Jurassic System of Russia: Problems of Stratigraphy and Palaeogeography. Fifth All Russian Meeting. Tyumen', September 23–27, 2013, Ekaterinburgpp. 249–251 (in Russian).
Sheridan, R.E., 1997. Pulsation tectonics as a control on the dispersal and assembly of supercontinents. J. Geodyn. 23, 173–196. http://dx.doi.org/10.1016/S0264-3707(96)00047-6.
Shurygin, B.N., Dzyuba, O.S., 2015. The Jurassic/Cretaceous boundary in northern Siberia and Boreal–Tethyan correlation of the boundary beds. Russ. Geol. Geophys. 56, 652–662. http://dx.doi.org/10.1016/j.rgg.2015.03.013.
Shurygin, B.N., Dzyuba, O.S., Izokh, O.P., Kosenko, I.N., Kuznetsov, A.B., 2015. Isotope markers (C, O, Sr) of the Jurassic–Cretaceous boundary beds in Boreal regions (Maurynya section, Western Siberia). In: Zakharov, V.A., Rogov, M.A., Ippolitov, A.P. (Eds.), Jurassic System of Russia: Problems of stratigraphy and paleogeography. Sixth All Russian Meeting. September 15–20, 2015, Scientific Materials, Makhachkalapp. 318–320 (in Russian).
Simms, M.J., Chidlaw, N., Morton, N., Page, K.N., 2004. British Lower Jurassic stratigraphy. In: Geological Conservation Review Series, No. 30. Joint Nature Conservation Committee, Peterborough (458 pp).
Smirnova, S.B., Shubin, S.V., Barskov, I.S., 1999. Spore and pollen assemblages from the bordering Middle and Upper Jurassic strata in the Central and Southern Moscow syneclise. Mosc. Univ. Geol. Bull. 54, 34–41.
Ullmann, C.V., Korte, C., 2015. Diagenetic alteration in low-Mg calcite from macrofossils: a review. Geol. Q. 59, 3–20. http://dx.doi.org/10.7306/gq.1217.
Ullmann, C.V., Hesselbo, S.P., Korte, C., 2013. Tectonic forcing of Early to Middle Jurassic seawater Sr/Ca. Geology 41, 1211–1214. http://dx.doi.org/10.1130/G34817.1.
Van der Meer, D.G., Zeebe, R.E., Van Hinsbergen, D.J.J., Sluijs, A., Spakman, W., Torsvik, T.H., 2014. Plate tectonic controls on atmospheric CO_2 levels since the Triassic. Proc. Natl. Acad. Sci. U. S. A. 111, 4380–4385. http://dx.doi.org/10.1073/pnas.1315657111.
Van der Vyver, C.P., 1986. The Stratigraphy and Ammonite Faunas of the Lower Kimmeridgian of Britain. University of Wales, Cardiff (unpublished PhD thesis. 550 pp.).
Vašiček, Z., Skupien, P., 2014. Recent discoveries of Tithonian ammonites in the Štramberk limestone (Kotouč quarry, Outer Western Carpathians). Ann. Soc. Geol. Pol. 84, 131–141.
Veizer, J., 1974. Chemical diagenesis of belemnite shells and possible consequences for paleotemperature determinations. N. Jb. Geol. Paläont. A. 147, 91–111.
Veizer, J., 1983. Chemical diagenesis of carbonates: theory and trace element technique. In: Arthur, M.A., Anderson, T.F., Kaplan, I.R., Veizer, J., Land, L.S. (Eds.), Stable Isotopes in Sedimentary Geology. SEPM Short Course No. 10, Dallaspp. 3-1–3-100.
Vishnevskaya, V.S., Baraboshkin, E.Yu., 2001. New data on biostratigraphy of the Volgian Stage lectostratotype near the Gorodishche village (Middle Volga Region). Stratigr. Geol. Correl. 9, 491–500.
Vollstaedt, H., Eisenhauer, A., Wallmann, K., Böhm, F., Fietzke, J., Liebetrau, V., Krabbenhöft, A., Farkaš, J., Tomašovych, A., Raddatz, J., Veizer, J., 2014. The Phanerozoic $\delta^{88/86}$Sr record of seawater: New constraints on past changes in oceanic carbonate fluxes. Geochim. Cosmochim. Acta 128, 249–265. http://dx.doi.org/10.1016/j.gca.2013.10.006.
Wierzbowski, H., 2002. Detailed oxygen and carbon isotope stratigraphy of the Oxfordian in Central Poland. Int. J. Earth Sci. (Geol. Rundsch.) 91, 304–314. http://dx.doi.org/10.1007/s005310100217.
Wierzbowski, H., 2004. Carbon and oxygen isotope composition of Oxfordian–Early Kimmeridgian belemnite rostra: palaeoenvironmental implications for Late Jurassic seas. Palaeogeogr. Palaeoclimatol. Palaeoecol. 203, 153–168. http://dx.doi.org/10.1016/S0031-0182(03)00673-4.
Wierzbowski, H., 2013. Strontium isotope composition of sedimentary rocks and its application to chemostratigraphy and palaeoenvironmental reconstructions. In: Annales Universitatis Mariae Curie-Skłodowska, Lublin – Polonia, Section AAA – Physica 68, pp. 23–37.
Wierzbowski, H., 2015. Seawater temperatures and carbon isotope variations in central European basins at the Middle–Late Jurassic transition (Late Callovian–Early Kimmeridgian). Palaeogeogr. Palaeoclimatol. Palaeoecol. 440, 506–523. http://dx.doi.org/10.1016/j.palaeo.2015.09.020.
Wierzbowski, H., Joachimski, M., 2007. Reconstruction of late Bajocian-Bathonian marine palaeoenvironments using carbon and oxygen isotope ratios of calcareous fossils from the Polish Jura Chain (central Poland). Palaeogeogr. Palaeoclimatol. Palaeoecol. 254, 523–540. http://dx.doi.org/10.1016/j.palaeo.2007.07.010.
Wierzbowski, A., Matyja, B.A., 2014. Ammonite biostratigraphy in the Polish Jura sections (central Poland) as a clue for recognition of the uniform base of the Kimmeridgian Stage. Vol. Jur. 12, 45–98.
Wierzbowski, H., Dembicz, K., Praszkier, T., 2009. Oxygen and carbon isotope composition of Callovian–Lower Oxfordian (Middle–Upper Jurassic) belemnite rostra from central Poland: a record of a Late Callovian global sea-level rise? Palaeogeogr. Palaeoclimatol. Palaeoecol. 283, 182–194. http://dx.doi.org/10.1016/j.palaeo.2009.09.020.
Wierzbowski, H., Anczkiewicz, R., Bazarnik, J., Pawlak, J., 2012. Strontium isotope variations in Middle Jurassic (Late Bajocian–Callovian) seawater: implications for Earth's tectonic activity and marine environments. Chem. Geol. 334, 171–181. http://dx.doi.org/10.1016/j.chemgeo.2012.10.019.
Wierzbowski, H., Rogov, M.A., Matyja, B.A., Kiselev, D., Ippolitov, A., 2013. Middle–Upper Jurassic (Upper Callovian–Lower Kimmeridgian) stable isotope and elemental records of the Russian Platform: indices of oceanographic and climatic changes. Glob. Planet. Chang. 107, 196–212. http://dx.doi.org/10.1016/j.gloplacha.2013.05.011.
Wierzbowski, H., Anczkiewicz, R., Bazarnik, J., Pawlak, J., 2014. Revised seawater strontium isotope curve for the Late Bajocian–Oxfordian (Middle–Late Jurassic). In:

Pandey, D.K., Fürsich, F.T., Alberti, M. (Eds.), 9th International Congress on the Jurassic System, Jaipur, India. Abstracts. Beringeria Special Issue 8, Erlangen, pp. 207–208.
Wierzbowski, A., Atrops, F., Grabowski, J., Hounslow, M., Matyja, B.A., Olóriz, F., Page, K., Parent, H., Rogov, M.A., Schweigert, G., Villaseñor, A.B., Wierzbowski, H., Wright, J.K., 2016. Towards a consistent Oxfordian/Kimmeridgian global boundary: current state of knowledge. Vol. Jur. 14, 15–50. http://dx.doi.org/10.5604/17313708.1201736.
Zeiss, A., 2003. The Upper Jurassic of Europe: its subdivision and correlation. Geol. Surv. Den. Greenl. 1, 75–114.